Study on the effects of Polyphyllin I and Curcumin on liver cancer based on the cross-action of ferroptosis and energy metabolism

Shuxian Yu
Hunan University of Chinese Medicine
Wenhui Gao
Hunan University of Chinese Medicine
Puhua Zeng (1060972939@qq.com)
Affiliated Hospital of Hunan Academy of Traditional Chinese Medicine
Mingxuan Lu
Hunan University of Chinese Medicine
Xiaoning Tan
Hunan Academy of Chinese Medicine Affiliated Hospital: Hunan University of Chinese Medicine Integrated Chinese Medicine Affiliated Hospital
Zhen Zhang
Hunan University of Chinese Medicine
Zhuo Liu
Hunan Academy of Chinese Medicine Affiliated Hospital: Hunan University of Chinese Medicine Integrated Chinese Medicine Affiliated Hospital
Zongwei Hou
Hunan University of Chinese Medicine
Jiyong Liu
Hunan University of Chinese Medicine

Research

Keywords: primary hepatic carcinoma, Polyphyllin I, curcumin, ferroptosis, energy metabolism, bioinformatics analysis

Posted Date: October 12th, 2021

DOI: https://doi.org/10.21203/rs.3.rs-929877/v1

Abstract

Background: To investigate the effect and mechanism of Polyphyllin I(PPI) and Curcumin(Cur) on human liver cancer HepG2 and HepG2.2.15 cells.

Methods: Download the hepatocellular carcinoma specimens and normal control specimens from the TCGA database, take the intersection with ferroptosis-related genes, and screen the differentially expressed ferroptosis genes; again, make the intersection with the selected differential genes related to energy metabolism; conduct survival analysis; construct prognosis Risk scoring model and evaluation of model performance; through molecular docking to verify the binding effect of PPI, Cur and Ribonucleoside-diphosphate reductase subunit M2(RRM2), SRC(SRC), Acetyl-CoA carboxylase alpha(ACACA) and other genes. Human hepatocellular carcinoma cells were cultured in vitro, PPI and Cur intervened, and Cell Counting Kit-8(CCK-8) was used to detect cell inhibition rate; FeRhoNox-1 fluorescent probe staining to observe the intracellular Fe 2+ status; lactate dehydrogenase (LDH) release Experiment to detect cell LDH release rate; JC-1 staining to detect mitochondrial membrane potential; reactive oxygen species(ROS) kit to detect ROS level;Western blotting (WB) to detect RRM2 and SRC , ACACA and other genes protein expression levels.

R**esults:** Through screening, 25 differential genes related to ferroptosis and energy metabolism in liver cancer were obtained;; through survival analysis, three ferroptosis-related genes, such as RRM2, SRC, and ACACA, were obtained the results showed that these three genes showed high expression and predicted poor overall survival(OS) and disease-free survival(DFS); molecular docking results showed that PPI, Cur It has good affinity with RRM2, SRC and ACACA. The results of in vitro experiments show that PPI and Cur inhibit cell proliferation in a concentration-dependent manner ($P < 0.01$). PPI and Cur can significantly increase the intracellular Fe2+ concentration, LDH release rate and intracellular ROS levels of HepG2, HepG2.2.15 ($P < 0.01$), and the effect on mitochondrial membrane potential was significantly lower than that of the blank group ($P < 0.01$), and significantly down-regulated the protein expression levels of RRM2, SRC, and ACACA ($P < 0.01$).

Conclusion: The high expression of RRM2, SRC, ACACA and other three genes related to ferroptosis and energy metabolism in liver cancer indicate poor OS and DFS; PPI and Cur can up-regulate the LDH release rate, ROS and Fe 2+ levels of liver cancer cells, and down-regulate the cell mitochondrial membrane potential and other methods to inhibit the proliferation of liver cancer cells; and down-regulate the expression of RRM2, SRC, ACACA and other proteins to affect the prognosis of liver cancer.

Introduction

Primary hepatic carcinoma (PHC) is one of the most common malignant tumors, a serious threat to health, and has a high morbidity and mortality rate worldwide [1]; Hepatitis B Virus (HBV) is an important inducement for the occurrence and development of primary liver cancer. In patients with liver cancer, hepatitis B virus infection accounts for 70% of the causes of liver cancer [2]. Therefore, studying the

prevention and treatment of HBV-related liver cancer has important guiding significance for the clinical treatment of liver cancer. As an important part of the comprehensive treatment of malignant tumors, traditional Chinese medicine has advantages in improving immunity, improving the quality of life, and prolonging the survival time of patients. It has played an active role in the clinical treatment of liver cancer [3]. At present, finding anti-tumor active ingredients from natural herbs is an important way for anti-cancer drug research.

PPI is a biologically active chemical substance isolated from the rhizomes of Chonglou. It has anti-tumor effects on a variety of tumor types [4,5]; studies have shown that PPI has an effect on the proliferation and migration of liver cancer cells, and can promote Apoptosis of liver cancer cells [6,7]. Cur is an acidic polyphenol compound extracted from the ginger family plant turmeric, which has the effects of inhibiting inflammation, anti-oxidation, and anti-rheumatoid [8]. Studies in recent years have shown that Cur has a clear anti-hepatocellular carcinoma effect, which can inhibit the growth and proliferation of liver cancer through a variety of ways, inhibit tumor angiogenesis, and induce tumor cell apoptosis [9,10].

Ferroptosis is an iron-dependent, a new type of programmed cell death that is different from apoptosis, cell necrosis, and autophagy. It is the generation of highly reactive and destructive ROS that is catalyzed by the overloaded free iron in the cell [11] , Activate the oxidative stress response, cause cell membrane rupture, mitochondrial cristae reduction or disappearance, lysosome or DNA damage and induce cell death [12]. The energy metabolism of liver cancer cells is an important way to supply energy for liver cancer to maintain its proliferation and migration, and mitochondria are the main places of energy metabolism [13]. Inducing the ferroptosis of liver cancer cells and destroying the balance of energy metabolism can effectively control the proliferation and metastasis of liver cancer. In this study, we screened genes that are commonly associated with ferroptosis and energy metabolism in liver cancer, and observed the effects of PPI and Cur on ferroptosis and energy metabolism in HBV-related liver cancer at the cellular level; hope to discover the potential mechanism of PPI and Cur in the treatment of liver cancer.

Materials And Methods

1.1 Screening of genes related to ferroptosis in liver cancer

Download the RNA sequencing data of the TCGA-LIHC cohort from the TCGA database (The Cancer Genome Atlas, https://portal.gdc.cancer.gov/), including 374 hepatocellular carcinoma specimens and 50 normal control specimens, and use R Language (R 3.6.3, https://www.r-project.org/) extracts and standardizes data. At the same time, 228 ferroptosis-related genes were obtained from FerrDb and previous studies (Annex 1), and the gene information in the expression matrix was crossed with ferroptosis-related genes to obtain a new ferroptosis-related gene expression matrix. Use "limma" R software for differential analysis and use the "edgeR" package to standardize expression profile data. The screening criteria for differential genes are: false discovery rate (FDR) <0.05 and |log2(Fold Change)|>1 .

Use the "ggplot2" and "pheatmap" packages to draw volcano maps and heat maps for the visualization of differential genes.

1.2 Screening of intersection genes related to ferroptosis and energy metabolism in liver cancer

Through literature search, 1394 energy metabolism-related genes (Annex 2) were obtained from the previously published literature, and the gene information in the expression matrix was crossed with the differentially expressed ferroptosis-related genes screened in 1.1 to obtain differential expression in liver cancer Of ferroptosis and energy metabolism related genes.

1.3 Survival analysis

The GEPIA database (http://gepia.cancer-pku.cn/index.html) was used to perform survival analysis on the 25 genes obtained from the 1.2 screening, and all patients were divided into high expression groups and low expression groups based on the median. Draw a survival curve, use log-rank test to compare the prognostic differences between the two groups of patients, and screen for genes with statistical differences.

1.4 Building a prognostic risk model

Use survival and survminer packages in R 4.0.5 software to perform single-factor COX regression analysis on the processed data to determine whether the three genes are related to prognosis, and then perform multi-factor COX regression analysis on genes with significant single-factor COX and based on the results Construct a prognostic risk scoring model. The risk score (RiskScore) calculation formula is: RiskScore=gene expression level 1×Coef1+gene expression level 2×Coef2+…+gene expression level n×Coefn (Coef: the regression coefficient of genes in multivariate Cox regression analysis). Use pheatmap and ggplot2 packages to visualize patient risk and gene expression involved in model construction.

1.5 Evaluation of the prognostic risk model

According to the risk value, the patients were divided into two groups with high and low risk. The R software "survival" package was loaded, and the survival curve of high and low risk scores, survival distribution maps and modeling gene expression heat maps were drawn according to the above groups. At the same time, the Kaplan-Meier survival curve was drawn using the "survminer" package of the R software to analyze and compare the OS of the two groups. Use the "timeROC" package to draw a receiver operator characteristic (ROC) curve. The area under the curve AUC will be used to evaluate the effectiveness of the model in predicting the prognosis of the patient. The higher the AUC, the better the model performance.

1.6 Correlation analysis of model clinical features

The independent risk factors identified through single-factor and multi-factor analysis were used as variables, and the ggpubr package was used to analyze the differences in risk scores between different clinical groups.

1.7 TIMER database analysis

TIMER (https://cistrome.shinyapps.io/timer/) uses RNA-seq expression profile data to detect the infiltration of immune cells in tumor tissues [14]. TIMER provides (CD4+T cells, CD8+T cells, B cells, macrophages, neutrophils and dendritic cells) the infiltration of 6 kinds of immune cells. The TIMER database was used to analyze the relationship between RRM2, SRC, ACACA gene expression and the infiltration of six immune cells in liver cancer. The search conditions are as follows: Click SCNA, in Cancer Types: select PHC; Gene symbol: input RRM2, SRC, ACACA, and click Submit.

1.8 Molecular docking

Use the RCSB PDB database (https://www.rcsb.org/) to download RRM2 (3bs9), SRC (4mxo), ACACA (4asi) co-crystals, and use Autodock tools to delete the excess water molecules and configuration of the co-crystals. Preparation of proteins such as body, adding hydrogen bonds; using ChemDraw.16 software to construct PPI, Cur, and calculating the lowest energy state; using Autodocl Vina 1.2.0 software for ligand processing and molecular docking procedures. Finally, PyMol 2.2.0 software was used to show the molecular docking simulation diagram of PPI and Cur with the above-mentioned proteins.

Cell In Vitro Experimental Verification

2.1 Materials

2.1.1 Cell Line

HepG2.2.15 cells were purchased from Guangzhou Genio Biotechnology Co., Ltd.; HepG2 cells for human liver cancer were gifted from the Tumor Research Institute of Xiangya Medical College, Central South University.

2.1.2 Drugs and main reagents

Polyphyllin I, curcumin, sorafenib, Erastin, Ferrostatin-1 (MCE company, batch numbers are: HY-N0047, HY-N0005, HY-10201, HY-15763, HY-100579); DMEM-high Sugar, fetal bovine serum, trypsin (0.25%), penicillin-streptomycin solution (GIBCO, USA, batch numbers: 11965092, A3160802, 25200056, 15240062); cell proliferation/toxicity detection kit (CCK-8 kit) (USA APExBIO, batch number: K1018); dimethyl sulfoxide DMSO (cell culture grade) (Beijing Soleibao Company, batch number: D8371); FeRhonox-1 iron ion (II) live cell imaging probe (Japan Goryo Company) , Lot number: GC901); lactate dehydrogenase (LDH) detection kit (Beijing Biolab Technology Co., Ltd., lot number: GL2055); JC-1 solution, reactive oxygen detection kit, DAPI staining solution (Shanghai Biyuntian Bio Technology Co., Ltd., batch number: C2005, S0033S, C1005) RIPA lysate (Shanghai Biyuntian Biotechnology Co., Ltd.,

batch number: P0013C); Phosphate Buffer solution (PBS) (Wuhan Punuosai Life Technology Co., Ltd., Lot number: PB180327); BCA protein quantification kit (Beijing Baierdi Biotechnology Co., Ltd., lot number: DEM109-500T); RRM2 antibody, SRC antibody, ACACA antibody (British Abcam, lot numbers: ab154964, ab47405, ab269273) .

2.1.3 Apparatus

370 series Steri-Cycle high temperature sterilization constant temperature CO2 incubator, 1300 Series A2 ultra-clean workbench, 3001 microplate reader (American Thermo Company); flow cytometer-CyFlow Cube6 (Guangzhou Jiyuan Biological Company); inverted microscope CKX41 (Olympus, Japan); DFM-60D inverted fluorescence microscope (Shanghai Caikang Optical Instrument Co., Ltd.); 1645052 high-current electrophoresis instrument, transfer tank, electrophoresis tank, ChemiDoc XRS gel imaging system (Bole, USA).

2.2 Method

2.2.1 Drug preparation

Polyphyllin I: Dissolve 5 mg of Polyphyllin I in 1ml of DMSO, and add 57ml of complete medium to obtain a mother liquor with a concentration of 100μmol/L when it is completely dissolved.

Curcumin: Dissolve 1 mg of curcumin in 1 ml of DMSO, and add 26 ml of complete medium to obtain a mother liquor with a concentration of 100 μmol/L when it is completely dissolved.

Sorafenib: Dissolve 1mg Sorafenib in 1ml DMSO, and add 106ml complete medium to obtain a mother liquor with a concentration of 100μmol/L when it is completely dissolved.

Erastin: Dissolve 1mg Erastin in 1ml DMSO, and add 17ml complete medium to obtain a mother liquor with a concentration of 100μmol/L when it is completely dissolved.

Store in a refrigerator at -80°C, and dilute with culture medium to the required concentration when used.

2.2.2 Cell culture and passage

HepG2 and HepG2.2.15 cells were both inoculated in complete medium (90% DMEM + 10% FBS + 1% double antibody) and incubated in a constant temperature 37°C 5% CO2 sterile incubator. The cell density reaches 80% for passage, digestion with 0.25% trypsin, complete medium is added to terminate the digestion, the cell suspension is pipetted and transferred to a centrifuge tube for centrifugation (1000 rpm, 3 min), and the supernatant is discarded and re-added to complete Divide the culture medium into new culture flasks to continue the culture. Take the cells whose growth cycle is in the logarithmic growth phase for further experiments.

2.2.3 CCK-8 method to detect cell viability

Take 0.25% trypsin to digest HepG2 and HepG2.2.15 cells, collect the cells after centrifugation for cell counting, and inoculate 100μL cell suspension per well (about 8x103 cells) in a 96-well plate. Incubate for 24 hours, add 10μLCCK-8 detection reagent to each well and continue to incubate for 2 hours. Use a microplate reader to detect the absorbance (A) at 450nm in each well. Graph PadPrism8.0 analyzes and calculates the half-inhibition rate concentration (1C50) of the drug. The experiment was repeated three times. In the next experiment, the concentration of the half inhibitory rate was used as the concentration to intervene the cells. In the experiment, the concentration of Ferrostatin-1 was 1μmol/L.

2.2.4 Cell grouping and administration

Take the HepG2 and HepG.2.15 cells in the logarithmic growth phase, wash 3 times with PBS buffer, digest with 0.25% trypsin, add complete medium to terminate the digestion, and place them in a 15ml centrifuge tube for cell centrifugation (1000rpm, 3min) , Discard the supernatant, pipette with complete medium to form a cell suspension, inoculate 3×105 cells per well in a 6-well plate, and incubate in an incubator for 24 hours; divide the cells into a blank group and PPI group, Cur group, sorafenib group, Erastin group, and Ferrostatin-1 group, they were observed and photographed under an optical microscope after 24 hours of drug intervention.

2.2.4 FeRhoNox-1 staining to observe the intracellular Fe^{2+} status

The HepG2 and HepG2.2.15 cell suspensions were inoculated in a 6-well plate with cell slides and placed in an incubator for 24 hours to adhere to the wall. Each drug group continued to intervene for 24 hours. Take out FeRhoNox-1 from the refrigerator, put it at room temperature for 30 min, centrifuge for 1 min, configure FeRhoNox-1 with DMSO solution as a storage solution with a final concentration of 1 mM, store at -20°C in the dark, and take PBS solution to store the solution when used Dilute to a final concentration of 5μM and preheat to 37°C. After 24 hours of drug intervention in the cells, aspirate the culture medium, wash with PBS buffer solution 3 times, add pre-heated FeRhoNox-1 staining solution, incubate in an incubator for 50 minutes, discard the staining solution, wash 3 times with PBS, and place Observe and take pictures under a fluorescence microscope.

2.2.5 Detection of LDH release rate

Take well-growing HepG2 and HepG2.2.15 cells in log phase, trypsin to digest the suspension, count the cells, inoculate them in a 12-well plate at a cell density of 5×104 cells/mL, 2 mL per well, each drug group Operate according to the instructions of the LDH kit after 24 hours of intervention. Measure the wavelength at 490 nm in the microplate reader. Cell LDH release rate (%)= (LDH activity in the medium/total LDH activity)×100%. The experiment was repeated three times.

2.2.6 Determination of intracellular ROS levels

The fluorescent probe DCFH-DA is used to detect the ROS level. By detecting the DCF fluorescence intensity in SKOV3 cells, the ROS level is evaluated. The DCF fluorescence intensity is directly

proportional to the intracellular ROS level. The pre-treatment method of cells is the same as that under 2.2. After 24 hours of intervention in each drug group, the cells are collected and suspended in diluted DCFH-DA (final concentration of 10 μm·L-1), incubated at 37 ℃ for 20 min, flow cytometry The instrument detects the intensity of DCF fluorescence (the fluorescence spectrum of DCF is very similar to FITC, so use FITC parameter settings to detect DCF). The experiment was repeated three times.

2.2.7 JC-1 staining to observe the mitochondrial membrane potential

Take well-growing HepG2 and HepG2.2.15 cells in the logarithmic phase, trypsin to digest the suspension, count the cells, inoculate them in a 12-well plate at a cell density of 5×104 cells/mL, 2 mL per well, each drug group After intervention for 24h, add the prepared JC-1 solution with a final mass concentration of 10μg/mL, incubate at 37°C for 30min in the dark, wash twice with PBS, add 200μL of new medium, and detect by flow cytometry. The experiment was repeated three times.

2.2.8 Western blot detection of protein expression of RRM2, SRC and ACACA

Each drug group was intervened for 24 hours, and the complete medium group was used as a blank control group to culture for 24 hours, lysed with RIPA lysis buffer (adding protease inhibitors), lysed on ice for 30 minutes, centrifuged to collect the supernatant, which is the total protein solution. The BCA kit detects the concentration of the collected protein. Add 5* reduced protein loading buffer to the protein solution at a ratio of 4:1, denature in a boiling water bath for 15 minutes, load 50μg protein per well, separate the protein by SDS-PAGE gel electrophoresis, transfer to PVDF membrane, and 5% degreasing The milk powder was sealed at room temperature for 2 h. Add RRM2 (1:1000), SRC (1:1000), ACACA (1:1000) according to the antibody instructions, and incubate in a shaker overnight at 4°C. Add TBST, place it on a decoloring shaker and wash the membrane three times, each time for 5 minutes, incubate for 1 hour at room temperature of the secondary antibody, add TBST again and wash the membrane three times, each time for 5 minutes. According to the ECL kit instructions, perform exposure and observe the protein expression, and use image J software to analyze the gray value. The experiment was repeated three times.

2.2.9 Statistical methods

Statistical analysis was performed using GraphPad Prism7 software. The measurement data is expressed as`x±s , and the *T* test is used for statistical analysis when comparing the results of the two groups, and the test level is α = 0.05.

Results

3.1 Screening of differential genes related to ferroptosis in liver cancer

A total of 69 ferroptosis-related genes were identified as differentially expressed genes in hepatocellular carcinoma, including 59 high-expressed genes and 10 low-expressed genes. The results are shown in Table 1, Figure 1.

Table 1
Differential genes related to ferroptosis in liver cancer

Gene	logFC	FDR	Gene	logFC	FDR
HSF1	1.46	6.21E-24	GLS2	-1.42	4.29E-15
SRXN1	2.04	1.65E-14	FTH1	1.04	3.31E-16
CS	1.36	1.16E-21	ABCC1	1.75	5.95E-06
EMC2	1.22	5.68E-23	ALOX15B	3.68	1.26E-06
SLC2A6	1.76	1.70E-07	ATF3	-1.19	2.65E-11
MAFG	1.98	6.22E-22	TFRC	1.58	6.95E-16
ASNS	2.36	4.96E-09	DDIT4	1.07	9.29E-05
DUSP1	-1.05	1.99E-13	AKR1C3	2.24	1.23E-22
MIOX	4.85	3.06E-11	AKR1C2	1.62	7.67E-06
TXNRD1	2.06	7.74E-17	AURKA	3.39	3.57E-26
PRKAA2	2.54	5.06E-10	NQO1	5.31	2.40E-15
PLIN2	-1.03	4.48E-12	EGLN2	1.25	1.11E-19
SLC7A11	4.89	8.32E-19	NRAS	1.04	2.92E-16
ALB	-1.27	4.10E-20	TUBE1	-1.20	5.06E-20
SLC1A5	1.69	0.005	SQSTM1	1.74	3.31E-16
DRD4	2.79	3.21E-14	ACSL4	2.66	9.25E-12
PML	1.06	3.89E-17	ACACA	1.49	3.50E-19
NF2	1.35	3.00E-23	HELLS	3.20	5.20E-23
ZFP36	-1.52	3.43E-17	ZNF419	1.17	2.55E-12
SLC7A5	1.03	0.031	YY1AP1	1.24	1.15E-22
SLC2A1	1.90	5.66E-05	STEAP3	-1.13	1.03E-18
FTL	1.01	1.20E-06	FADS2	1.06	0.013
FANCD2	2.95	5.83E-24	RPL8	1.74	3.08E-20
SQLE	2.29	2.22E-17	AIFM2	1.43	3.14E-20
HRAS	1.59	1.21E-23	MAPK3	1.38	1.68E-24
TAZ	1.68	1.32E-26	DDIT3	1.51	1.24E-16
CAV1	1.05	6.58E-09	GPX2	1.32	0.012
AKR1C1	1.22	0.0005	NNMT	-1.74	4.71E-17

Gene	logFC	FDR	Gene	logFC	FDR
MT1G	-1.93	3.33E-22	HSPB1	2.25	8.97E-23
SRC	1.86	4.81E-10	DNAJB6	1.17	1.12E-24
CDKN2A	4.65	4.70E-24	NCF2	1.05	0.014
SLC1A4	1.39	1.93E-14	CAPG	1.92	4.64E-11
HSPA5	1.07	5.37E-19	RRM2	3.76	1.12E-24
G6PD	3.37	1.06E-23	BAP1	1.06	1.64E-22
STMN1	2.83	1.11E-25			

3.2 Differential genes related to ferroptosis and energy metabolism in liver cancer

A total of 25 genes related to ferroptosis and energy metabolism were identified as differentially expressed genes in hepatocellular carcinoma, including 22 highly expressed genes and 3 low expressed genes. The results are shown in Table 2, Figure 2.

Table 2
Differential genes related to ferroptosis and energy metabolism in liver cancer

Gene	logFC	FDR	Gene	logFC	FDR
ASNS	2.36	4.96E-09	GLS2	-1.42	4.29E-15
TXNRD1	2.06	7.74E-17	ABCC1	1.75	5.95E-06
PRKAA2	2.54	5.06E-10	ALOX15B	3.68	1.26E-06
PLIN2	-1.03	4.48E-12	TFRC	1.58	6.95E-16
ALB	-1.27	4.10E-20	DDIT4	1.07	9.29E-05
SLC2A1	1.90	5.66E-05	AKR1C3	2.24	1.23E-22
SQLE	2.29	2.22E-17	AKR1C2	1.62	7.67E-06
TAZ	1.68	1.32E-26	ACSL4	2.66	9.25E-12
CAV1	1.05	6.58E-09	ACACA	1.49	3.50E-19
AKR1C1	1.22	0.0005	FADS2	1.06	0.013
SRC	1.86	4.81E-10	GPX2	1.32	0.012
HSPA5	1.07	5.37E-19	RRM2	3.76	1.12E-24
G6PD	3.37	1.06E-23			

3.3 Survival Analysis

The 25 genes were divided into high expression group and low expression group. The results showed that RRM2, SRC, ACACA and other genes OS and DFS were statistically different. The results are shown in Figure 3. The survival curve indicated that RRM2, SRC, and ACACA may be related to OS and DFS in liver cancer patients. The OS and DFS of the high expression group of RRM2, SRC, and ACACA were significantly lower than those of the low expression group (P<0.01 or P<0.05). These results suggest that RRM2 high expression of SRC and ACACA may indicate poor OS and DFS.

3.4 Cox Analysis And Risk Model Construction

Performing multivariate Cox regression analysis on RRM2, SRC, and ACACA, we finally obtained two ferroptosis and energy metabolism genes that are significantly related to the prognosis of liver cancer, which constitute the prognostic risk score model for liver cancer (Figure 4). Among them, the HR of RRM2 and SRC>1, suggesting that high expression is related to high risk.

3.5 Risk Model Performance Evaluation

According to the expression of RRM2, SRC and regression coefficients, the risk score of each liver cancer sample was calculated, and the patients were divided into a high-risk score group (N=171) and a low-risk score group (N=171). The visual analysis results show that red represents the high-risk score group, and blue represents the low-risk score group (Figure 5A). The high-risk score group had a lower proportion of deaths than the risk group, indicating that the high-risk score group was more likely to have a poor prognosis (Figure 5B). RRM2 and SRC were highly expressed in the high-risk score group, suggesting that high expression was positively correlated with high risk (Figure 5C); it was consistent with the survival analysis results in Figure 3A-3E. The KaplanMeier survival curve showed that patients with high-risk scores had lower OS and patients with lower-risk scores had lower OS, and there was a significant difference in OS between the two (P=0.004, Figure 5D). The ROC curve result is shown in Figure 5E, and the AUC is 0.751, which shows that the prediction model is more accurate.

3.6 Correlation Between Risk Score And Clinical Characteristics

Use the data of the TCGA-LIHC dataset to further study whether the model has predictive performance for patients with different clinical characteristics, including gender, age, tumor size, lymph node metastasis, tumor stage, EGFR gene mutation, ALK gene fusion, KRAS gene mutation And state of existence. Analysis results: patients aged ≤50 have a higher risk score than patients ≥65, and patients aged 50-65 have a higher risk score than patients ≥65, and there is a significant difference (P<0.05, Figure 6A); female patients are compared with men The risk score of patients is high and statistically different (P<0.05, Figure 6B); patients with grade G2 have higher risk scores than patients with G1, patients with G3 have higher risk scores than patients with G1, and patients with G4 have higher risk scores than patients with

G1. Patients with high risk score, G3 patients have higher risk scores than G2 patients, and G4 patients have higher risk scores than G2 patients, and the results are statistically significant (*P*□0.01 or *P*□0.05); patients with stage □ stage The risk score is higher than that of stage □ patients, and the risk score of stage □ patients is higher than that of stage □ patients. The result is statistically significant (*P*□0.01 or *P*□0.05); patients in T2 stage have higher risk scores than patients in T1, T3 stage patients have higher risk scores than T1 stage patients, and the results are statistically significant (*P*<0.01 or *P*<0.05); Nx stage patients have higher risk scores than N0 stage patients and have statistical significance *(P*<0.01); There were no significant differences in the risk scores of patients with M stage, with or without lymph node metastasis, with or without EGFR gene mutation, with or without ALK gene fusion, and with or without KRAS gene mutation. The above results indicate that the risk score is closely related to age, gender, grade classification, stage staging, T staging, and N staging.

3.7 The relationship between the expression of RRM2, SRC, ACACA and immune cell infiltration in liver cancer

The TIMER database was used to analyze the correlation between the expression of RRM2, SRC, ACACA and immune cell infiltration in liver cancer. The results showed that RRM2, SRC gene expression and cell purity, B cells, CD8+ T cells, macrophages, neutrophils, dendrites The level of immune infiltration of cells has a certain correlation. The expression of ACACA gene has a certain correlation with the level of immune infiltration of cell purity, B cells, CD4+T cells, macrophages, neutrophils, and dendritic cells; RRM2, SRC 2. ACACA may be involved in the immune infiltration process of liver cancer cells. The results were statistically significant (*P*<0.01 or *P*<0.05). See Figure 7.

3.7 Molecular docking of PPI, Cur and RRM2, SRC, ACACA

The molecular docking of PPI and Cur with RRM2, SRC, ACACA was carried out through Autodock 4.2.1 software, and the visual analysis of molecular docking was carried out through Pymol 2.3.2 software. The results are shown in Figure 8. PPI and Cur have good affinity with RRM2, SRC and ACACA.

3.9 Inhibition of each drug group on HepG2 and HepG2.2.15 cells

CCK-8 method test results showed that PPI and Cur at different concentrations compared with the blank group had inhibitory effects on HepG2 and HepG2.2.15 cells (*P*<0.01), and the inhibitory effect was significantly dependent on the concentration of the drug. In order to screen the optimal inhibitory concentration of each drug group on HepG2 and HepG2.2.15 cells, IC50 was further calculated, and the results are shown in Figure 9.

3.10 The effect of each drug group on the proliferation of HepG2 and HepG2.2.15 cells

Under normal culture conditions, the HepG2 parent cells are arranged in an epithelial-like monolayer, with fusiform or irregular polygonal shapes, adherent growth, uniform size, and clear edges. HepG2.2.15 cells integrated with the HBV whole genome are used to grow in clusters and appear as a single layer. Or double-layered, with clear outline and a round shape. Compared with the blank group, the numbers of the

two kinds of cells were significantly reduced after treatment with different drugs, the shape gradually became round, and the medium contained a lot of cell debris. The results are shown in Figure 10.

3.10 The effect of each drug group on Fe $^{2+}$ of HepG2 and HepG2.2.15 cells

The results of FeRhoNox-1 staining showed that compared with the control group, the fluorescence intensity of PPI and Cur was significantly increased, indicating that PPI and Cur could significantly increase the intracellular Fe^{2+} concentration of HepG2 and HepG2.2.15 (P<0.01). The results are shown in Figures 11 and 12.

3.11 The effect of each drug group on the LDH release rate of HepG2 and HepG2.2.15 cells

Compared with the blank group, the LDH release rate of the PPI and Cur group was significantly increased (P 0.01), indicating that PPI and Cur can increase the permeability of HepG2 and HepG2.2.15 cell membranes and induce cell damage. See Figure 13.

3.12 The effect of each drug group on the intracellular ROS levels of HepG2 and HepG2.2.15

Compared with the blank group, the PPI and Cur groups can significantly increase the intracellular ROS levels of HepG2 and HepG2.2.15 (P<0.01). The results are shown in Figures 14, 15.

3.13 The influence of each drug group on the mitochondrial membrane electricity of HepG2 and HepG2.2.15 cells

Flow cytometry detection after JC-1 staining showed that after the intervention of the PPI and Cur drug groups, the influence of the mitochondrial membrane potential of HepG2 and HepG2.2.15 cells was significantly lower than that of the blank group, and there was a statistical difference (P< 0.01 or P 0.05), the results are shown in Figures 16, 17.

3.14 The effect of each drug group on the expression of RRM2, SRC and ACACA protein in HepG2 and HepG2.2.15 cells

In HepG2 and HepG2.2.15 cells, the protein expression levels of RRM2, SRC and ACACA were significantly down-regulated in the control group compared with the blank group, and the difference was statistically significant (P<0.01 or P<0.05). See Figures 18 and 19.

Discussion

Primary liver cancer grows rapidly, the disease progresses quickly, the degree of malignancy is high, and it is easy to invade and migrate. HBV is one of the important reasons for inducing liver cancer. Relevant studies have shown that in China, the incidence of hepatocellular carcinoma (HCC) accounts for 55% of the world's rate, and about 90% are HBV-related liver cancer [15].

Ferroptosis is a cell-regulated necrosis characterized by lipid oxidation and iron-dependent pathways, which is different from traditional caspase-dependent apoptosis and cell necrosis with established pathways [11]. Energy metabolism of tumor cells is the main way to provide energy for tumors to maintain tumor proliferation and migration [13].

Rhizoma Paridis is the rhizome of a flower of Liliaceae Rhizoma Paridis, which has the functions of clearing away heat and toxins, reducing swelling and pain, cooling the liver and relieving convulsions. Modern pharmacological studies have shown that the drug has a wide range of pharmacological activities such as hemostasis, anti-tumor, immune regulation, and cardiovascular effects [16]. The main chemical component of Chonglou is steroidal saponins, which account for about 80% of the total number of compounds. Among them, saponins of Chonglou is its anti-tumor active ingredient. Many scholars have found that saponins of PPI have shown obvious anti-tumor effect in the experiments [4–7]. Cur is a class of diketone compounds extracted from the roots of turmeric plants such as turmeric and zedoary. It has anti-tumor, anti-HIV and anti-oxidant pharmacological effects [8]. Cur has a wide range of anti-tumor mechanisms, and its molecular mechanism of anti-tumor angiogenesis has been confirmed [9, 10].

In this study, RNA sequencing data related to liver cancer was collected through the TCGA database and intersected with ferroptosis and energy metabolism-related genes respectively. 25 differential genes related to ferroptosis and energy metabolism in liver cancer were obtained, which were further screened by survival analysis; finally 3 were obtained OS and DFS have statistically different genes; RRM2, SRC, ACACA, among which RRM2, also known as ribonucleotide reductase subunit M2, is one of the important components of ribonucleotide reductase, which participates in DNA Biological processes such as the synthesis and repair of tumor cells affect tumor cell proliferation, differentiation, invasion and migration. Current research reports that RRM2 is relatively highly expressed in breast cancer [17, 18], lung adenocarcinoma (LUAD) [19, 20], and cervical cancer [21, 22], and it is also expressed in a variety of tumor cell proliferations. It plays an important role in the process of invasion, invasion and migration.Src kinase is the main product of the proto-oncogene c-Src and is a non-receptor tyrosine protein kinase. There are currently 11 family members discovered, and Src is currently one of the most studied members [23]. Src consists of SH4 domain, specific fragments, SH3 domain, SH2 domain, linker, SH1 domain (protein tyrosine kinase domain) and carboxy-terminal regulatory tail [24]. Src plays an important role in cell processes such as cell proliferation, differentiation, movement and localization. Studies have shown that activation of the Src pathway is involved in the progression of malignant tumors such as colon cancer [25], prostate cancer [26], ovarian cancer [27], breast cancer [28], and lung cancer [29]. Acetyl Coenzyme A Carboxylase (ACAC) is a family of biotin-containing enzymes, including ACACA and ACACB, which catalyze the production of malonyl-CoA from acetyl-Coenzyme A and have a limiting effect on the synthesis of fatty acids in the cell. Studies have shown that the expression of phosphorylated ACACA protein is related to the tumor grade and stage of breast cancer [30], and there is also overexpression of ACACA in liver cancer [31]. The results of this study show that the high expression of RRM2, SRC, and ACACA may indicate poor OS and DFS, and through Cox analysis, risk model construction and risk model performance evaluation, it is known that the high expression of RRM2 and SRC is related to high risk. AUC of 0.751 indicates this prediction The accuracy of the model is high.

The energy metabolism of tumor cells is one of the characteristics that distinguish tumor cells from normal cells. The growth of tumor cells depends on glycolysis and generates a small amount of energy under the action of LDH to meet metabolic needs [32]. In this study, PPI and Cur can increase the LDH release rate of HepG2 and HepG2.2.15 cells, indicating that PPI and Cur can increase cell membrane permeability and induce cell damage. ROS is a by-product of cell normal oxygen metabolism, and it plays a great role in cell signal transduction and maintaining the constancy of the body. Excessive ROS levels can damage the structure of cells and genes. Studies have found that mitochondria are the main targets of ROS strikes. At this point, the accumulation of ROS in cells promotes the decrease of mitochondrial membrane potential, leading to mitochondrial dysfunction, which affects the energy metabolism of tumors [33]. In addition, ferroptosis is a cellular regulatory necrosis characterized by iron and ROS dependence. Up-regulation of intracellular ROS can induce cellular ferroptosis pathways. The results of this study show that PPI and Cur can increase the level of ROS in HepG2 and HepG2.2.15 cells, and down-regulate the mitochondrial membrane potential of HepG2 and HepG2.2.15 cells. In addition, this study also found that PPI and Cur can also up-regulate Fe^{2+} levels in HepG2 and HepG2.2.15 cells, which may induce cell ferroptosis.

In summary, three differential genes that are commonly associated with ferroptosis and energy metabolism in liver cancer were screened out through bioinformatics analysis, namely: RRM2, SRC, and ACACA. Survival analysis results show that high expression of RRM2, SRC, and ACACA may indicate poor OS, DFS; Cox analysis and risk model performance evaluation show that the high expression of RRM2 and SRC is related to high risk. In vitro experiments show that PPI and Cur can inhibit cell proliferation by increasing the LDH release rate, intracellular ROS level, intracellular Fe^{2+} level, and down-regulating the cell mitochondrial membrane potential in HepG2 and HepG2.2.15 cells; the specific mechanism of action may be related to PPI, Cur can down-regulate the protein expression levels of genes such as RRM2, SRC, ACACA, and this result is consistent with the results of bio-information analysis.

Abbreviations

PPI Polyphyllin I

Cur Curcumin

LDH lactate dehydrogenase

ROS reactive oxygen species

WB Western blotting

PHC Primary hepatic carcinoma

HBV Hepatitis B Virus

FDR false discovery rate

ROC receiver operator characteristic

OS overall survival

DFS disease-free survival

HCC hepatocellular carcinoma

LUAD lung adenocarcinoma

ACACA Acetyl-CoA carboxylase alpha

ACAC Acetyl Coenzyme A Carboxylase

RRM2 Ribonucleoside-diphosphate reductase subunit M2

SRC SRC

CCK8 Cell Counting Kit-8

Declarations

ETHICS APPROVAL AND CONSENT TO PARTICIPATE

Not applicable.

HUMAN AND ANIMAL RIGHTS

No animals/humans were used for studies that are base of this research.

CONSENT FOR PUBLICATION

Not applicable.

AVAILABILITY OF DATA AND MATERIALS

Not applicable.

FUNDING

This work was supported by the National Natural Science Foundation of China(81603603,82074425);Natural Science Foundation of Hunan Province (2021JJ30417); Key Scientific Research Project of Hunan Provincial Department of Education(19A369), Key Issues of Hunan Provincial Administration of Traditional Chinese Medicine(201803), Hunan Science and Technology Planning Project(2016SK2051) and Postgraduate Research and Innovation Project of Hunan University of Traditional Chinese Medicine (CX20190569).

Authors' contributions

Shuxian Yu, Wenhui Gao, Zongwei Hou, etc. did the in vitro experiment part of the manuscript; Shuxian Yu and Mingxuan Lu jointly completed the bioinformatics analysis in the manuscript; Shuxian Yu wrote the article; Puhua Zeng proposed research ideas and designed research plans; Wenhui Gao , Mingxuan Lu, Xiaoning Tan, Zhen Zhang, etc. conducted statistical analysis on the data; Zhuo Liu, Zongwei Hou and Jiyong Liu and others translated the manuscript.

CONFLICT OF INTEREST

The authors declare no conflict of interest, financial or otherwise.

ACKNOWLEDGEMENTS

Declared none.

References

1. Celsa C, Cabibbo G, Pagano D. **di** Marco V, Cammà C, Gruttadauria S. Sicily Network for Liver Cancer: A Multidisciplinary Network Model for the Management of Primary Liver Tumors. J Laparoendosc Adv Surg Tech A. 2020 **Oct**;30(10):1048–53. **doi**: 10.1089/lap.2020.0471. **Epub 2020 Jul 13. PMID: 32668179**.
2. Lebossé F, Zoulim F. **Vaccination contre le virus de l'hépatite B et prévention du cancer du foie [Hepatitis B vaccine and liver cancer]**. **Bull Cancer**. **2021 Jan**;**108**(1):**90-101**. **French**. **doi**: 10.1016/j.bulcan.2020.10.014. **Epub 2020 Dec 25**. **PMID**: **33358507**.
3. Wang K, Chen Q, Shao Y, Yin S, Liu C, Liu Y, Wang R, Wang T, Qiu Y, Yu H. **Anticancer activities of TCM and their active components against tumor metastasis**. **Biomed Pharmacother**. 2021 **Jan**;**133**:**111044**. **doi**: 10.1016/j.biopha.2020.111044. **Epub 2020 Dec 11**. **PMID**: **33378952**.
4. Lai L, Shen Q, Wang Y, Chen L, Lai J, Wu Z, Jiang H. **Polyphyllin I reverses the resistance of osimertinib in non-small cell lung cancer cell through regulation of PI3K/Akt signaling**. Toxicol Appl Pharmacol. 2021 May 15;**419**:**115518**. **doi**: **10.1016/j.taap.2021.115518**. **Epub 2021 Apr 1. PMID: 33812963**.
5. Yu S, Gao W, Zeng P, Chen C, Zhang Z, Liu Z, Liu J. Exploring the effect of Gupi Xiaoji Prescription on hepatitis B virus-related liver cancer through network pharmacology and in vitro experiments. Biomed Pharmacother. 2021 **Jul**;139:111612. 10.1016/j.biopha.2021.111612. **Epub 2021 Apr 26. PMID: 33915505**.. ;. **doi**.
6. Liu J, Man S, Liu Z, Ma L, Gao W. **A synergistic antitumor effect of polyphyllin I and formosanin C on hepatocarcinoma cells**. **Bioorg Med Chem Lett**. **2016 Oct 15**;**26**(**20**):**4970-4975**. **doi**: 10.1016/j.bmcl.2016.09.005. **Epub 2016 Sep 3**. **PMID**: **27623551**.
7. Yu S, Gao W, Zeng P, Chen C, Liu Z, Zhang Z, Liu J. **Exploring the effect of Polyphyllin I on hepatitis B virus-related liver cancer through network pharmacology and in vitro experiments**. **Comb Chem High**

Throughput Screen. 2021 **Aug 16**. **doi**: 10.2174/1386207324666210816141436. **Epub ahead of print**. **PMID**: **34397325**.

8. Dei Cas M, Ghidoni R. **Dietary Curcumin**: **Correlation between Bioavailability and Health Potential**. **Nutrients**. 2019 **Sep 8**;**11**(**9**):**2147**. **doi**: 10.3390/nu11092147. **PMID**: **31500361**; **PMCID**: **PMC6770259**.
9. Deng Z, Xu XY, Yunita F, Zhou Q, Wu YR, Hu YX, Wang ZQ, Tian XF. **Synergistic anti-liver cancer effects of curcumin and total ginsenosides**. **World J Gastrointest Oncol**. **2020 Oct 15**;**12**(**10**):**1091-1103**. **doi**: 10.4251/wjgo.v12.i10.1091. **PMID**: **33133379**; **PMCID**: **PMC7579727**.
10. Ren B, Luo S, Tian X, Jiang Z, Zou G, Xu F, Yin T, Huang Y, Liu J. **Curcumin inhibits liver cancer by inhibiting DAMP molecule HSP70 and TLR4 signaling**. **Oncol Rep**. 2018 **Aug**;**40**(**2**):**895-901**. **doi**: 10.3892/or.2018.6485. **Epub 2018 Jun 11**. **PMID**: **29901164**.
11. Sui X, Zhang R, Liu S, Duan T, Zhai L, Zhang M, Han X, Xiang Y, Huang X, Lin H, Xie T. **RSL3 Drives Ferroptosis Through GPX4 Inactivation and ROS Production in Colorectal Cancer**. Front Pharmacol. 2018 Nov 22;**9**:**1371**. **doi**: 10.3389/fphar.2018.01371. **PMID: 30524291; PMCID: PMC6262051**.
12. Sumneang N, Siri-Angkul N, Kumfu S, Chattipakorn SC, Chattipakorn N. **The effects of iron overload on mitochondrial function, mitochondrial dynamics, and ferroptosis in cardiomyocytes**. Arch Biochem Biophys. 2020 Feb 15;**680**:**108241**. **doi**: 10.1016/j.abb.2019.108241. **Epub 2019 Dec 28. PMID: 31891670**.
13. Guerra F, Arbini AA, Moro L. Mitochondria and cancer chemoresistance. Biochim Biophys Acta Bioenerg. 2017 **Aug**;1858(8):686–99. 10.1016/j.bbabio.2017.01.012. **Epub 2017 Feb 1. PMID: 28161329**.. ;). **doi**.
14. Li T, Fan J, Wang B, Traugh N, Chen Q, Liu JS, Li B, Liu XS. **TIMER**: **A Web Server for Comprehensive Analysis of Tumor-Infiltrating Immune Cells**. **Cancer Res**. **2017 Nov 1**;**77**(**21**):**e108-e110**. **doi**: 10.1158/0008-5472.CAN-17-0307. **PMID**: **29092952**; **PMCID**: **PMC6042652**.
15. Lu T, Yang Q, Li M, Zhang J, Zou J, Huang L, Lin J, Jin H, He J. HBV infection and extra-hepatic cancers in adolescents and 20s: A retrospective study in China. Cancer Epidemiol. 2018 **Aug**;55:149–55. 10.1016/j.canep.2018.05.012. **Epub 2018 Jun 30. PMID: 29980026**.. ;. **doi**.
16. Man S, Chai H, Cui J, Yao J, Ma L, Gao W. Antitumor and anti-metastatic mechanisms of Rhizoma paridis saponins in Lewis mice. Environ Toxicol. 2018 **Feb**;33(2):149–55. 10.1002/tox.22501. **Epub 2017 Nov 17. PMID: 29148169**.. ;). **doi**.
17. Li S, Mai H, Zhu Y, Li G, Sun J, Li G, Liang B, Chen S. **MicroRNA-4500 Inhibits Migration, Invasion, and Angiogenesis of Breast Cancer Cells via RRM2-Dependent MAPK Signaling Pathway**. Mol Ther Nucleic Acids. 2020 Sep 4;**21**:**278-289**. **doi**: 10.1016/j.omtn.2020.04.018. **Epub 2020 May 4. PMID: 32615527; PMCID: PMC7330432**.
18. Zhuang S, Li L, Zang Y, Li G, Wang F. RRM2 elicits the metastatic potential of breast cancer cells by regulating cell invasion, migration and VEGF expression via the PI3K/AKT signaling. Oncol Lett. 2020 **Apr**;19(4):3349–55. 10.3892/ol.2020.11428. **Epub 2020 Mar 3. PMID: 32256828; PMCID: PMC7074627**.. ;). **doi**.

19. Ma C, Luo H, Cao J, Gao C, Fa X, Wang G. **Independent prognostic implications of RRM2 in lung adenocarcinoma**. **J Cancer**. **2020 Oct 17**;**11**(**23**):**7009-7022**. **doi**: 10.7150/jca.47895. **PMID**: **33123291**; **PMCID**: **PMC7592001**.
20. Jin CY, Du L, Nuerlan AH, Wang XL, Yang YW, Guo R. **High expression of RRM2 as an independent predictive factor of poor prognosis in patients with lung adenocarcinoma**. **Aging** (**Albany NY**). 2020 **Dec 19**;**13**(**3**):**3518-3535**. **doi**: 10.18632/aging.202292. **Epub 2020 Dec 19**. **PMID**: **33411689**; **PMCID**: **PMC7906179**.
21. Wang J, Yi Y, Chen Y, Xiong Y, Zhang W. **Potential mechanism of RRM2 for promoting Cervical Cancer based on weighted gene co-expression network analysis**. **Int J Med Sci**. **2020 Aug 29**;**17**(**15**):**2362-2372**. **doi**: 10.7150/ijms.47356. **PMID**: **32922202**; **PMCID**: **PMC7484645**.
22. Zhao H, Zheng GH, Li GC, Xin L, Wang YS, Chen Y, Zheng XM. Long noncoding RNA LINC00958 regulates cell sensitivity to radiotherapy through RRM2 by binding to microRNA-5095 in cervical cancer. J Cell Physiol. 2019 **Dec**;234(12):23349–59. 10.1002/jcp.28902. **Epub 2019 Jun 6. PMID: 31169309**.. (:. **doi**.
23. Belli S, Esposito D, Servetto A, Pesapane A, Formisano L, Bianco R. **c-Src and EGFR Inhibition in Molecular Cancer Therapy**: **What Else Can We Improve? Cancers** (**Basel**). 2020 **Jun 7**;**12**(**6**):**1489**. **doi**: 10.3390/cancers12061489. **PMID**: **32517369**; **PMCID**: **PMC7352780**.
24. Meng Y, Pond MP, Roux B. **Tyrosine Kinase Activation and Conformational Flexibility**: **Lessons from Src-Family Tyrosine Kinases**. **Acc Chem Res**. **2017 May 16**;**50**(**5**):**1193-1201**. **doi**: 10.1021/acs.accounts.7b00012. **Epub 2017 Apr 20**. **PMID**: **28426203**; **PMCID**: **PMC6602532**.
25. Lin X, Wang G, Liu P, Han L, Wang T, Chen K, Gao Y. Gallic acid suppresses colon cancer proliferation by inhibiting SRC and EGFR phosphorylation. Exp Ther Med. 2021 **Jun**;21(6):638. 10.3892/etm.2021.10070. **Epub 2021 Apr 16. PMID: 33968169; PMCID: PMC8097205**.. ;). **doi**.
26. Lu Y, Dong B, Xu F, Xu Y, Pan J, Song J, Zhang J, Huang Y, Xue W. **CXCL1-LCN2 paracrine axis promotes progression of prostate cancer via the Src activation and epithelial-mesenchymal transition**. Cell Commun Signal. 2019 Sep 10;**17**(**1**):**118**. **doi**: 10.1186/s12964-019-0434-3. **PMID: 31500632; PMCID: PMC6734451**.
27. Yang Y, Liu J, Qian X, Li Y, Wang Y, Xu X. **miR-485-5p improves the progression of ovarian cancer by targeting SRC in vitro and in vivo**. Neoplasma. 2020 **Sep**;67(**5**):**1022-1031**. **doi**: 10.4149/neo_2020_190927N979. **Epub 2020 Jun 16. PMID: 32538666**.
28. Song L, Liu Z, Hu HH, Yang Y, Li TY, Lin ZZ, Ye J, Chen J, Huang X, Liu DT, Zhou J, Shi Y, Zhao H, Xie C, Chen L, Song E, Lin SY, Lin SC. **Proto-oncogene Src links lipogenesis via lipin-1 to breast cancer malignancy**. Nat Commun. 2020 Nov 17;**11**(**1**):**5842**. **doi**: 10.1038/s41467-020-19694-w. **PMID: 33203880; PMCID: PMC7672079**.
29. Hsu PC, Yang CT, Jablons DM, You L. **The Crosstalk between Src and Hippo/YAP Signaling Pathways in Non-Small Cell Lung Cancer** (**NSCLC**). **Cancers** (**Basel**). 2020 **May 26**;**12**(**6**):**1361**. **doi**: 10.3390/cancers12061361. **PMID**: **32466572**; **PMCID**: **PMC7352956**.

30. Rios Garcia M, Steinbauer B, Srivastava K, Singhal M, Mattijssen F, Maida A, Christian S, Hess-Stumpp H, Augustin HG, Müller-Decker K, Nawroth PP, Herzig S, Berriel Diaz M. **Acetyl-CoA Carboxylase 1-Dependent Protein Acetylation Controls Breast Cancer Metastasis and Recurrence**. Cell Metab. 2017 Dec 5;**26**(**6**):**842-855.e5**. **doi**: **10.1016/j.cmet.2017.09.018**. **Epub 2017 Oct 19. PMID: 29056512**.
31. Lally JSV, Ghoshal S, DePeralta DK, Moaven O, Wei L, Masia R, Erstad DJ, Fujiwara N, Leong V, Houde VP, Anagnostopoulos AE, Wang A, Broadfield LA, Ford RJ, Foster RA, Bates J, Sun H, Wang T, Liu H, Ray AS, Saha AK, Greenwood J, Bhat S, Harriman G, Miao W, Rocnik JL, Westlin WF, Muti P, Tsakiridis T. Harwood HJ **Jr**, Kapeller R, Hoshida Y, Tanabe KK, Steinberg GR, Fuchs BC. **Inhibition of Acetyl-CoA Carboxylase by Phosphorylation or the Inhibitor ND-654 Suppresses Lipogenesis and Hepatocellular Carcinoma**. **Cell Metab**. **2019 Jan 8**;**29**(**1**):**174-182.e5**. **doi**: **10.1016/j.cmet.2018.08.020**. **Epub 2018 Sep 20**. **PMID**: **30244972**; **PMCID**: **PMC6643297**.
32. Deckers EA, Kruijff S, Brouwers AH. **van der** Steen K, Hoekstra HJ, Thompson JF, Vállez García D, Wevers KP. **The association between active tumor volume, total lesion glycolysis and levels of S-100B and LDH in stage IV melanoma patients**. Eur J Surg Oncol. 2020 **Nov**;46(**11**):**2147-2153**. **doi**: **10.1016/j.ejso.2020.07.011**. **Epub 2020 Jul 27. PMID: 32819759**.
33. Zheng T, Chen HXYSXZKJLLXBJPY. Anticancer effects of curzerenone against drug-resistant human lung carcinoma cells are mediated via programmed cell death, loss of mitochondrial membrane potential, ROS, and blocking the ERK/MAPK and NF-κB signaling pathway. J BUON. 2019 **May-Jun**;24(3):907–12. **PMID: 31424641**.

Figures

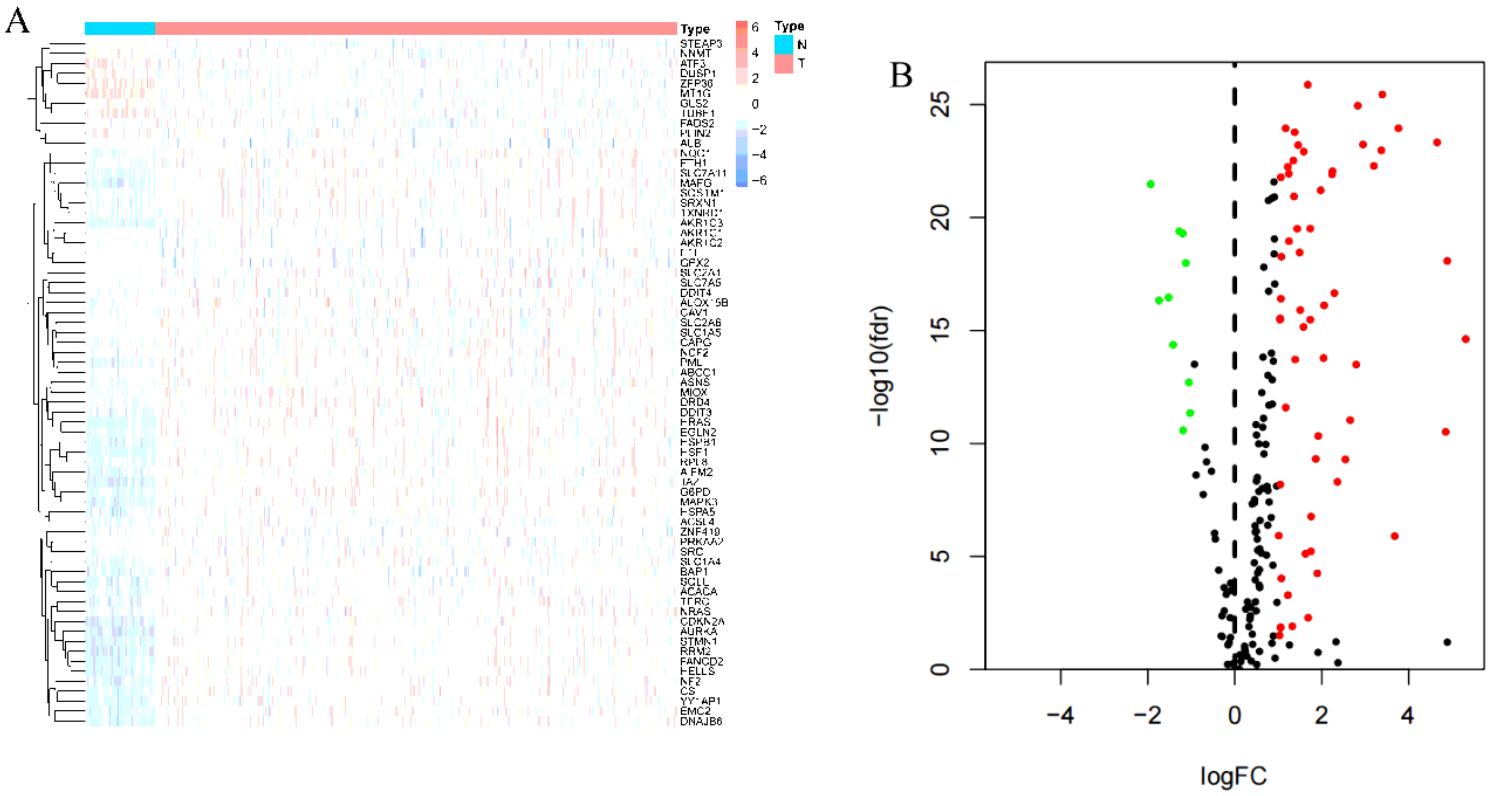

Figure 1

Differentially expressed ferroptosis-related genes. (A) Shows the expression level of ferroptosis genes differentially expressed in tumors (T) and normal tissues (N). The redder the color means the higher the expression level, and the greener the expression level is lower; (B) shows all iron The value of FDR and LogFC of death-related genes, each point represents an ferroptosis-related gene, green and red are different ferroptosis-related genes, the left side represents LogFC<0 (where green <-1), the right side represents LogFC >0 (where red >1)

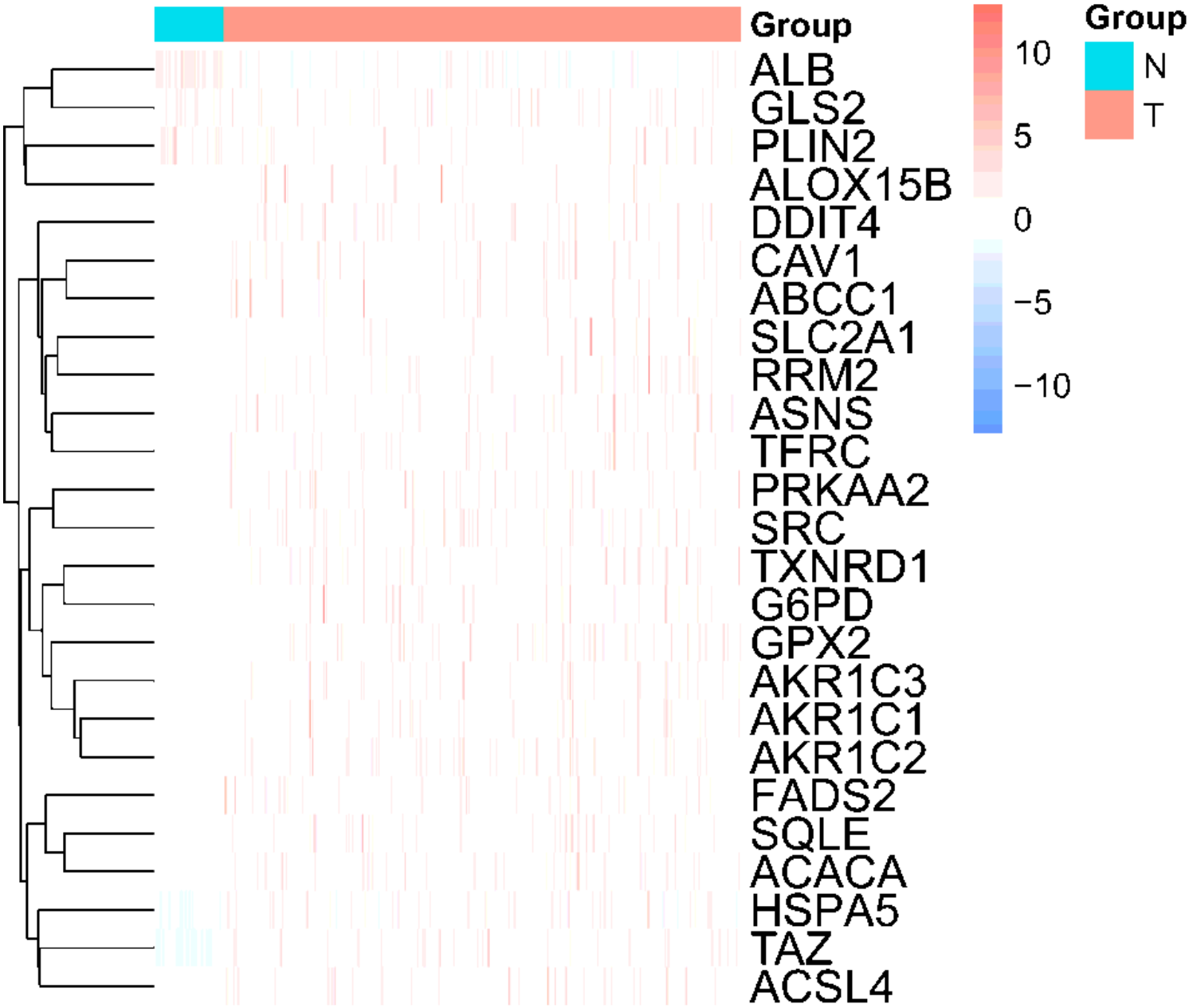

Figure 2

Differentially expressed genes related to ferroptosis and energy metabolism in liver cancer.Shows the expression levels of ferroptosis genes that are differentially expressed in tumors (T) and normal tissues (N). The more red the color indicates the higher the expression, and the greener the expression is, the lower the expression.

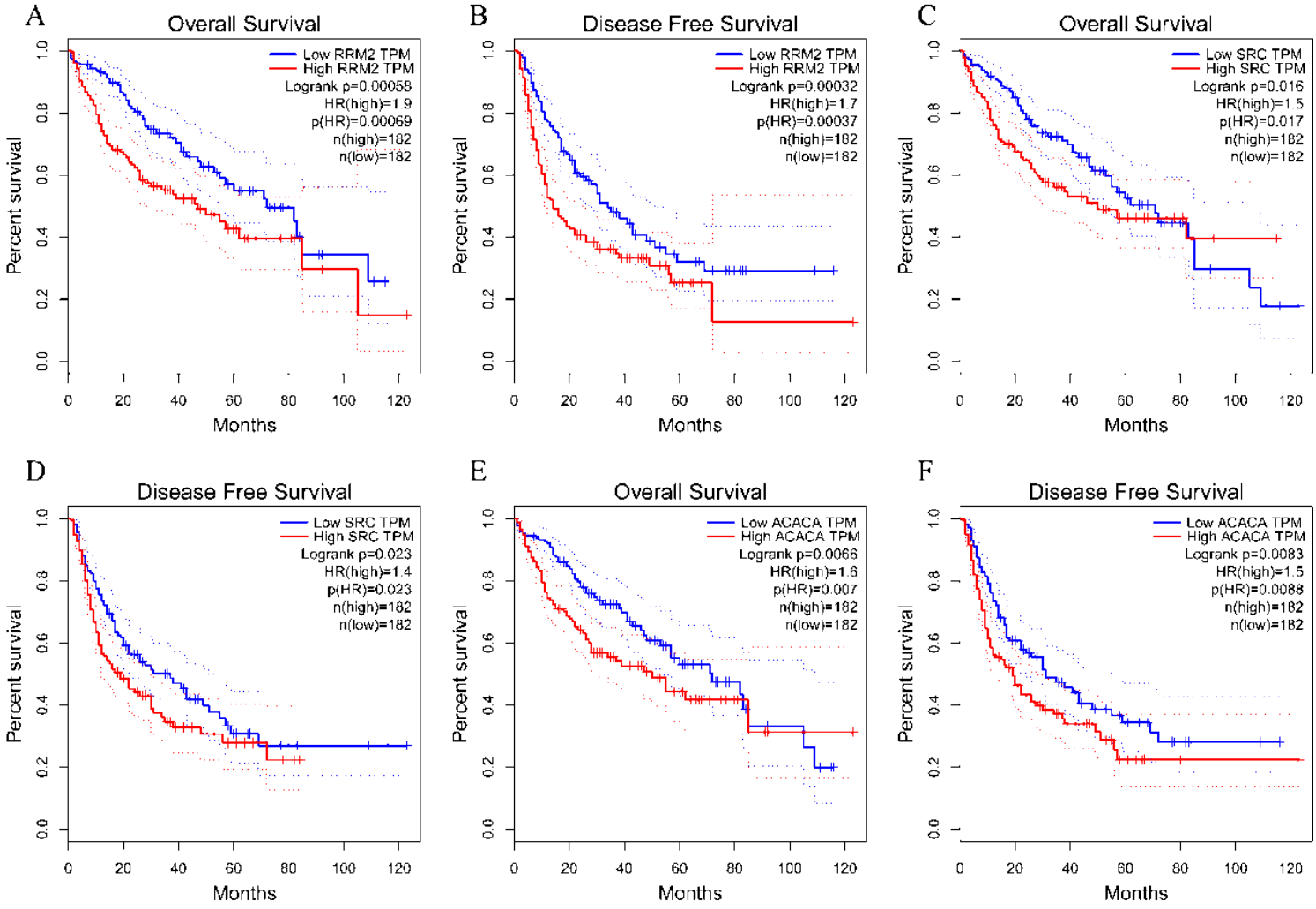

Figure 3

The relationship between the expression levels of RRM2, SRC, ACACA and the overall survival (OS) and disease-free survival (DFS) of patients with liver cancer.A. The relationship between RRM2 expression level and OS in liver cancer patients; B. The relationship between RRM2 expression level and DFS in liver cancer patients; C. The relationship between SRC expression level and OS in liver cancer patients; D. The relationship between SRC expression level and DFS in liver cancer patients; E. The relationship between the expression level of ACACA and OS in patients with liver cancer; F. The relationship between the expression level of ACACA and DFS in patients with liver cancer.

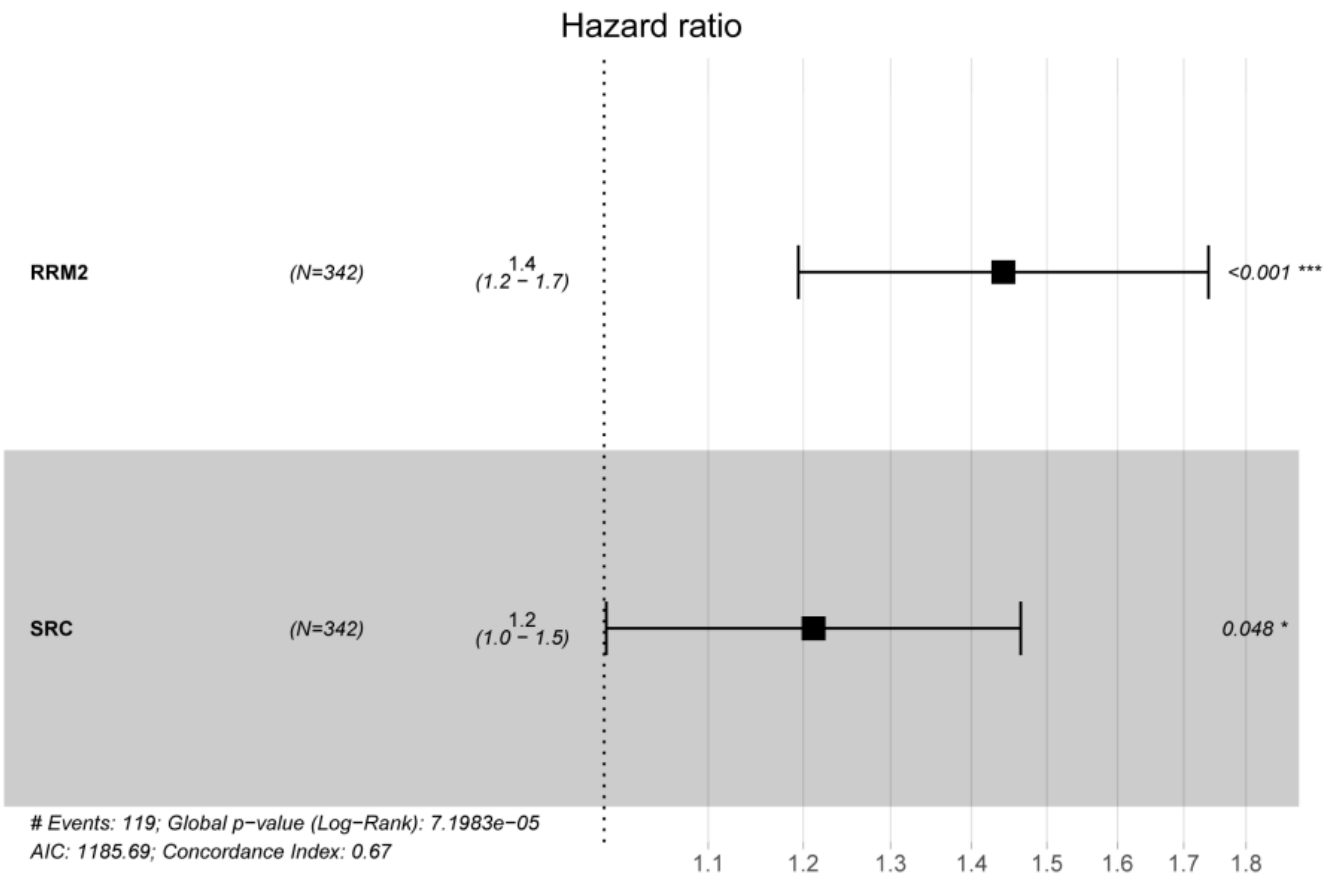

Figure 4

Forest plot of multivariate Cox regression analysis results

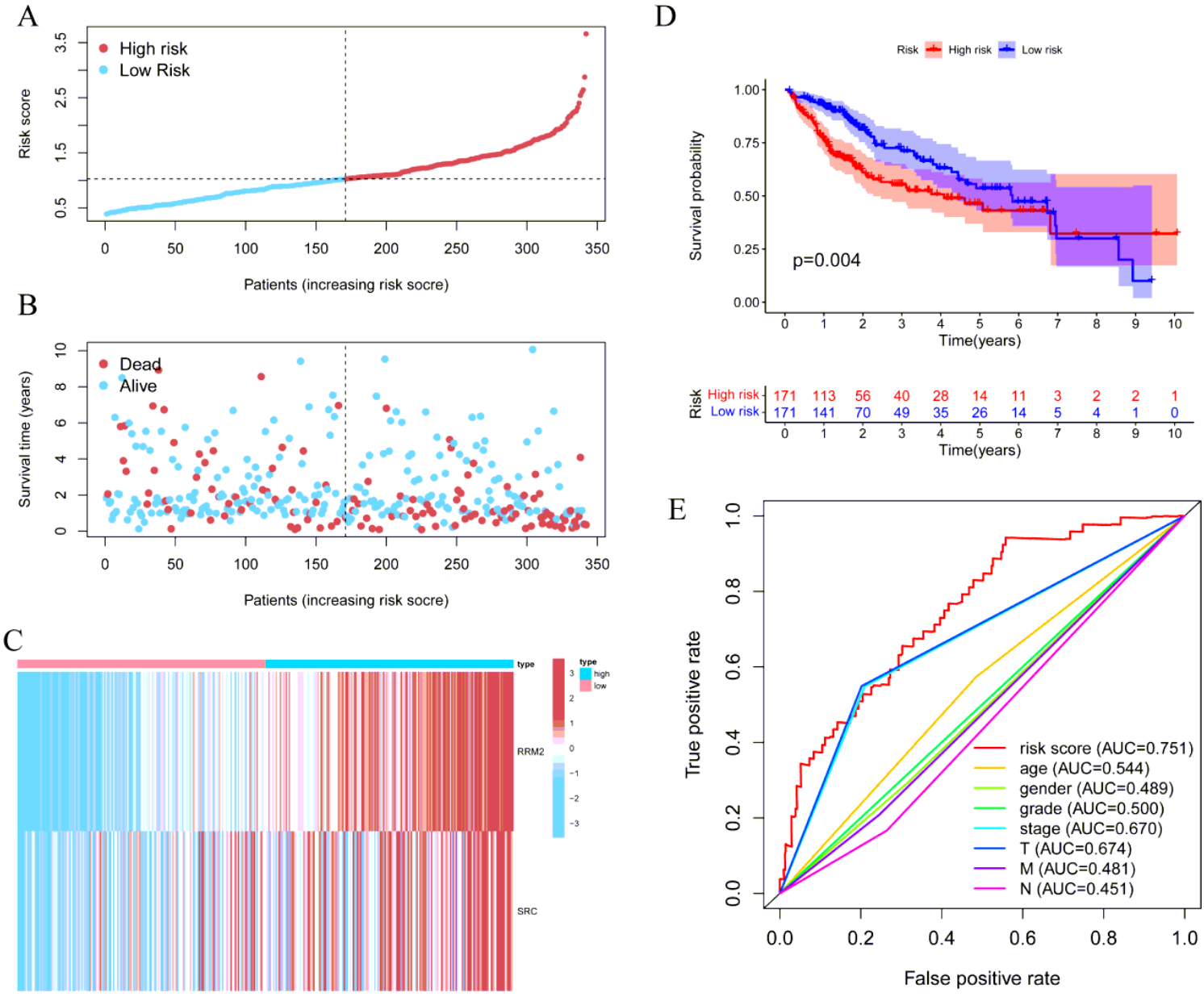

Figure 5

Performance evaluation of the prognostic risk scoring model. A: risk curve; B: survival status diagram; C: modeling gene expression heat map; D: Kaplan-Meier survival curve; E: ROC curve

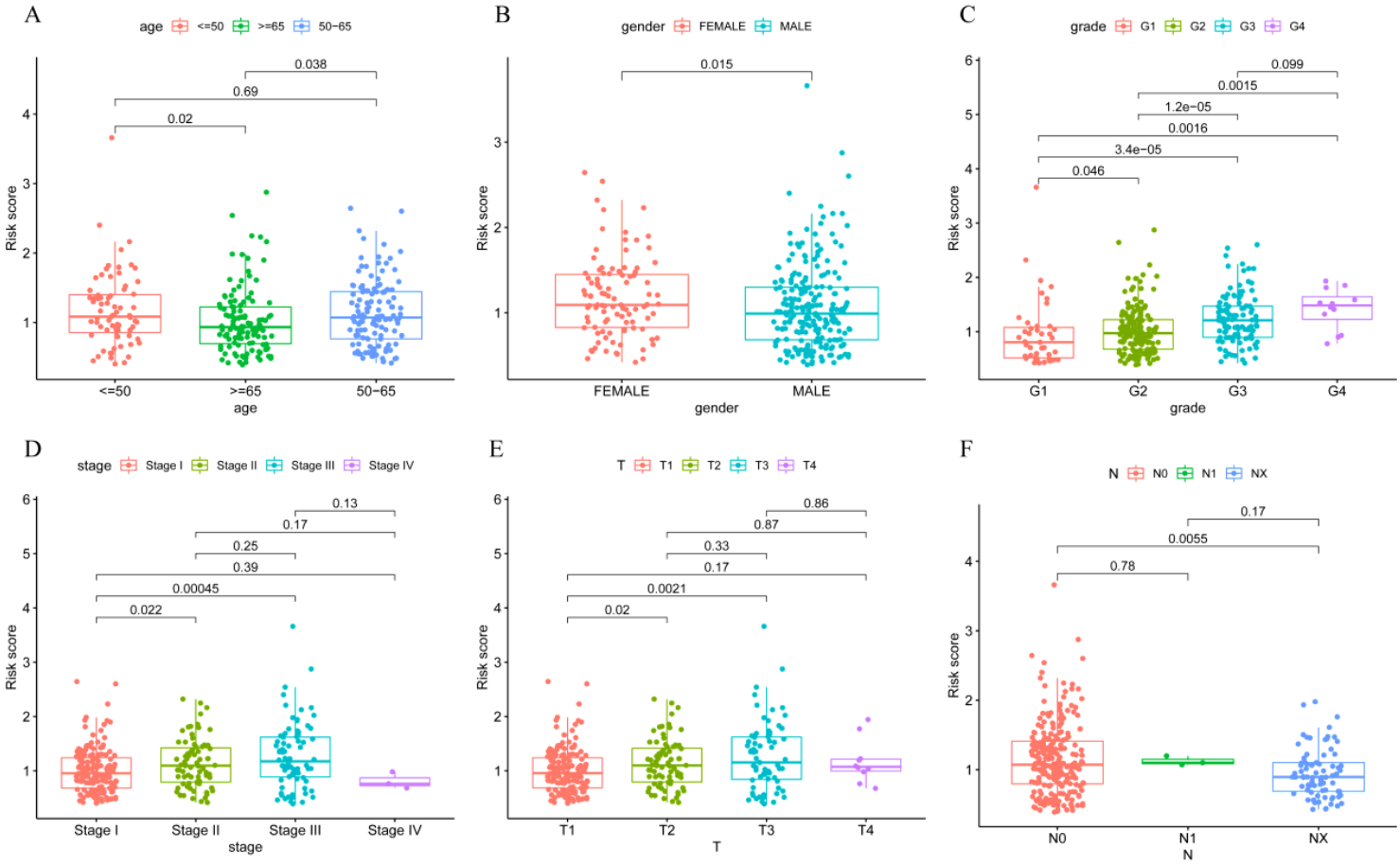

Figure 6

Clinical correlation analysis.A. Relationship between risk score and age; B. Relationship between risk score and gender; C. Relationship between risk score and grade; D. Relationship between risk score and stage staging; E. Relationship between risk score and T stage; F. The relationship between risk score and N staging.

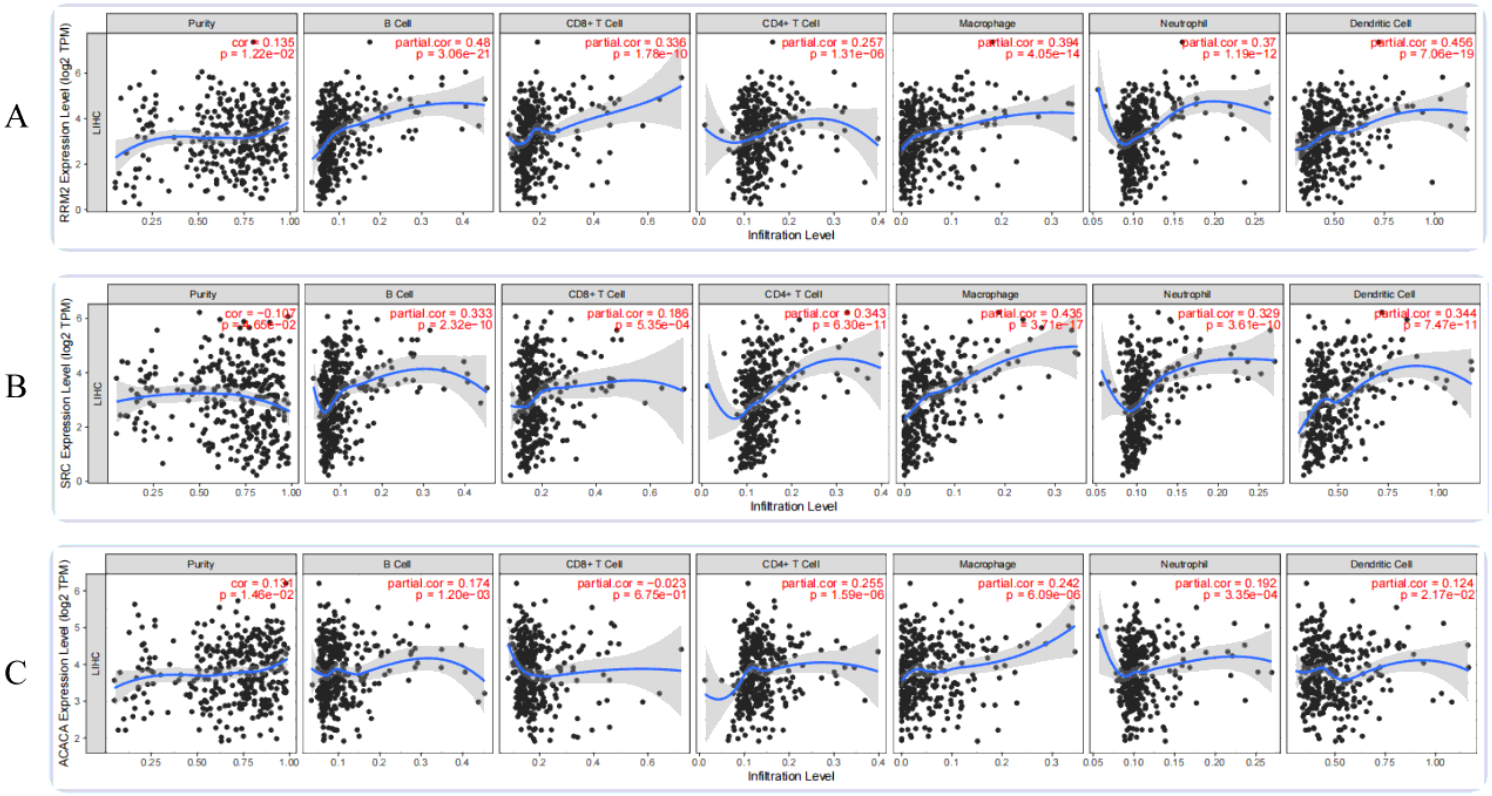

Figure 7

The relationship between RRM2, SRC, ACACA expression and liver cancer immune cell infiltration.A. The relationship between RRM2 expression and immune cell infiltration in liver cancer; B. The relationship between SRC expression and immune cell infiltration in liver cancer; C. The relationship between ACACA expression and immune cell infiltration in liver cancer.

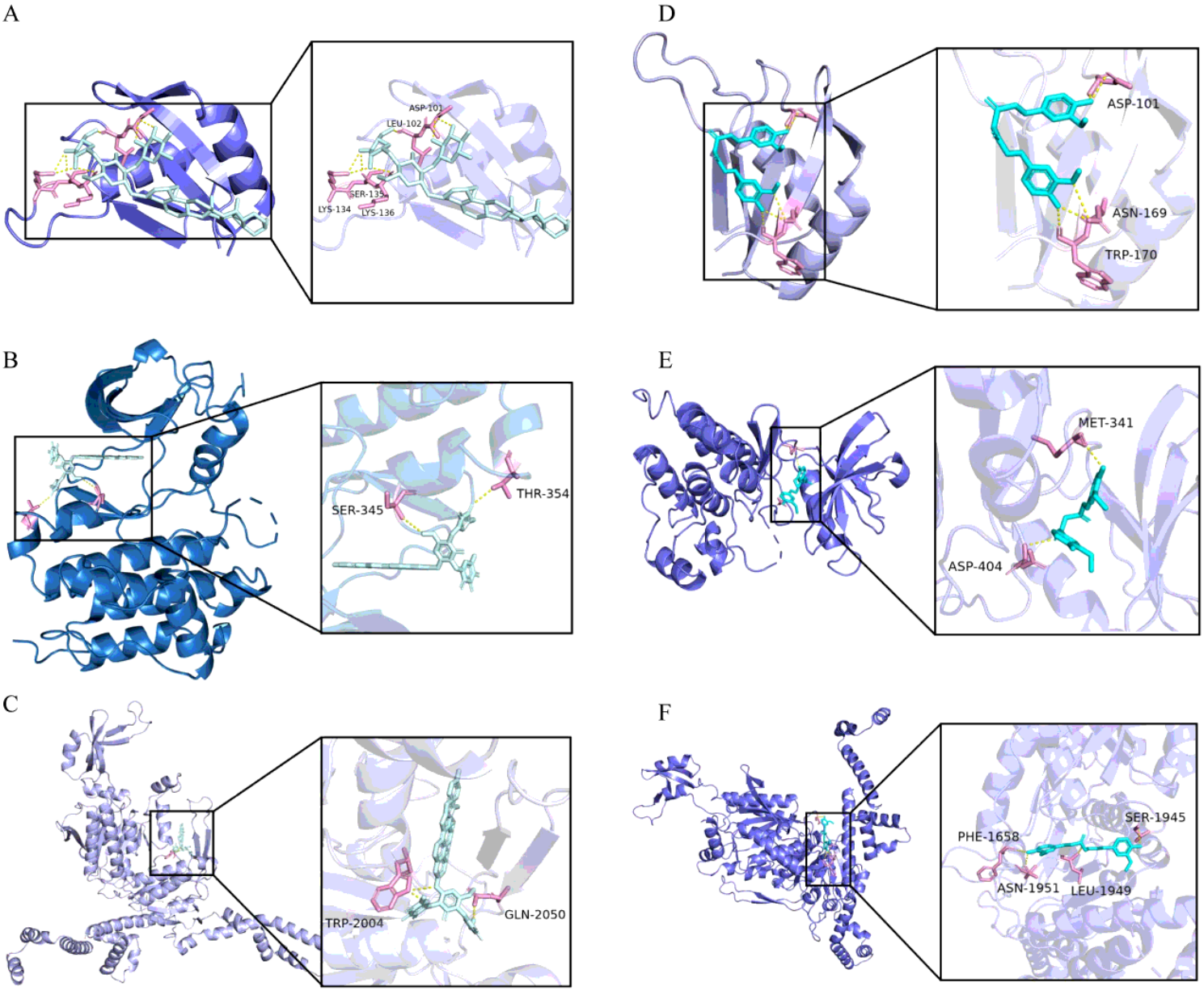

Figure 8

The molecular docking diagram of PPI, Cur and RRM2, SRC, ACACA A. Docking of PPI and RRM2; B. Docking of PPI and SRC; C. Docking of PPI and ACACA; D. Docking of Cur and RRM2; E. Docking of Cur and SRC Molecular docking; F. Cur and ACACA molecular docking

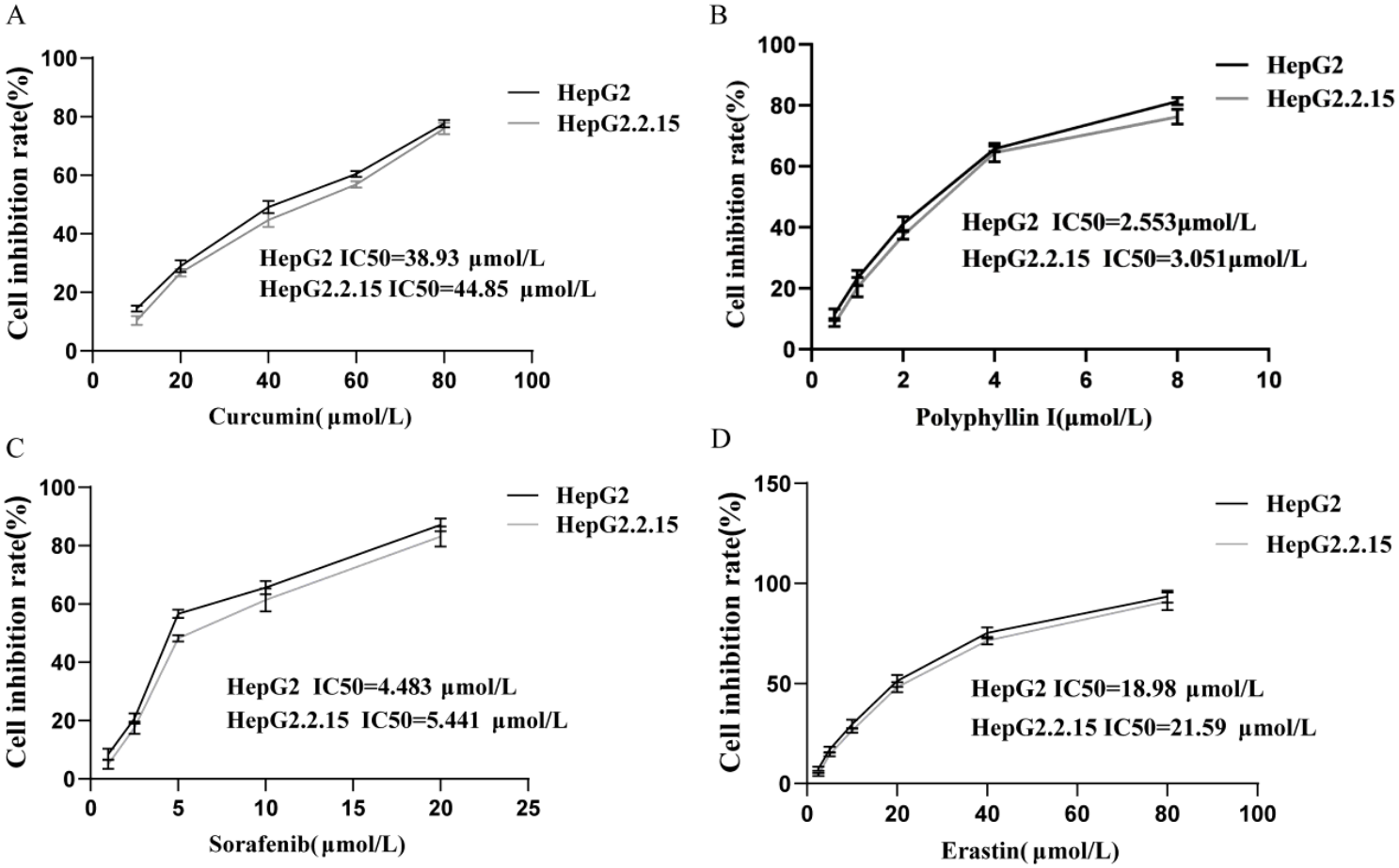

Figure 9

The inhibitory effect of each drug group on HepG2 and HepG2.2.15 cells

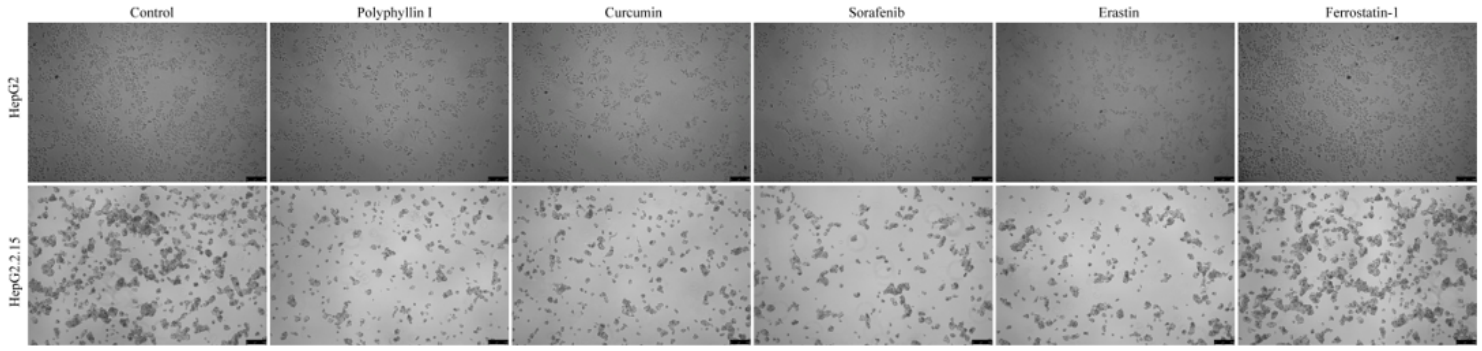

Figure 10

The effect of each drug group on the proliferation of HepG2 and HepG2.2.15 cells (x10 times). A. Blank group; B. PPI; C. Cur; D. Sorafenib; E. Erastin; F. Ferrostatin-1

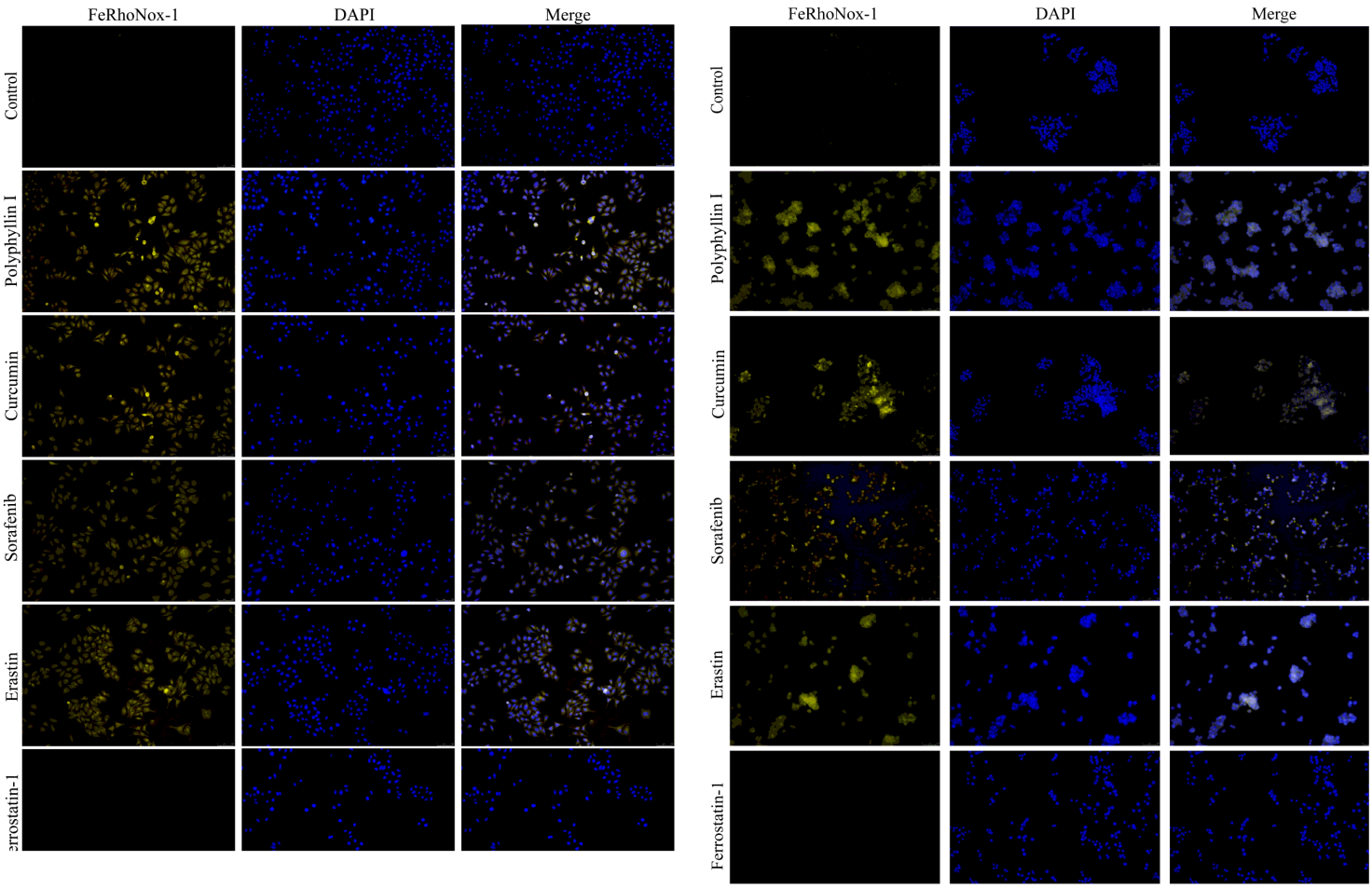

Figure 11

The effect of each drug group on Fe2+ in HepG2 and HepG2.2.15 cells (x10 times)

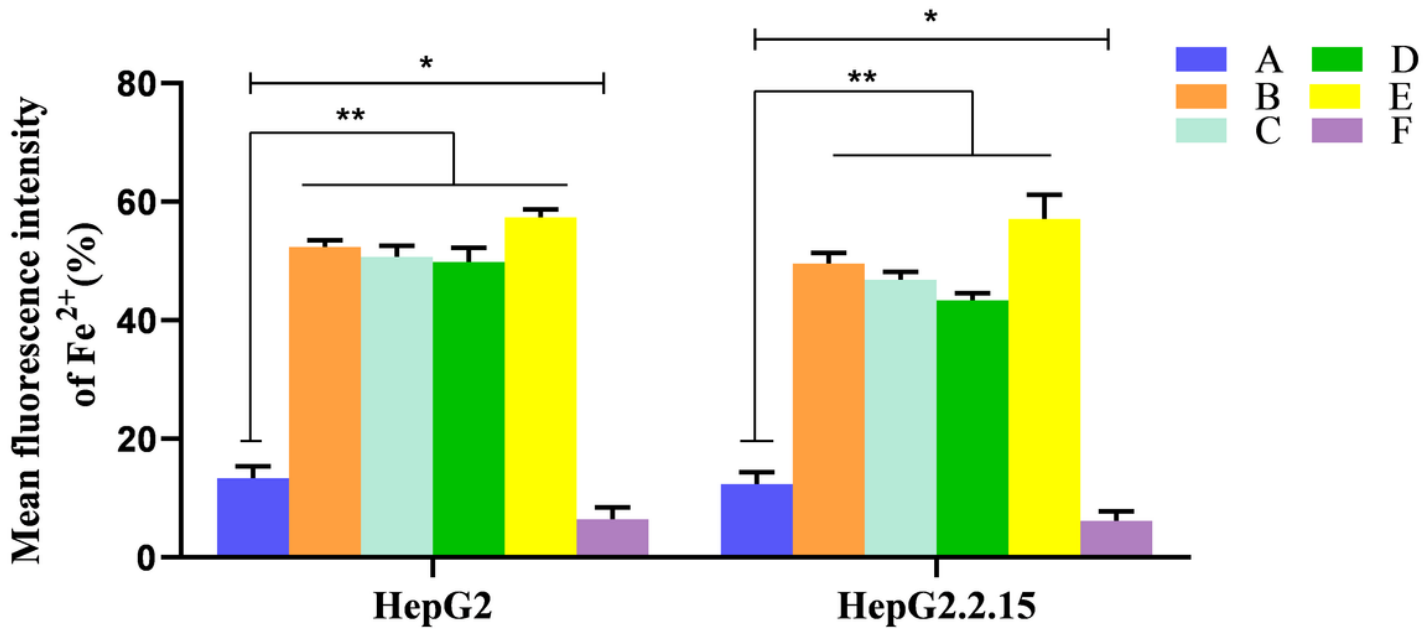

Figure 12

The average fluorescence intensity of Fe2+ staining in HepG2 and HepG2.2.15 cells (`x±s□n=3).A. Blank group; B. PPI; C. Cur; D. Sorafenib; E. Erastin; F. Ferrostatin-1; **P<0.01, *P<0.05.

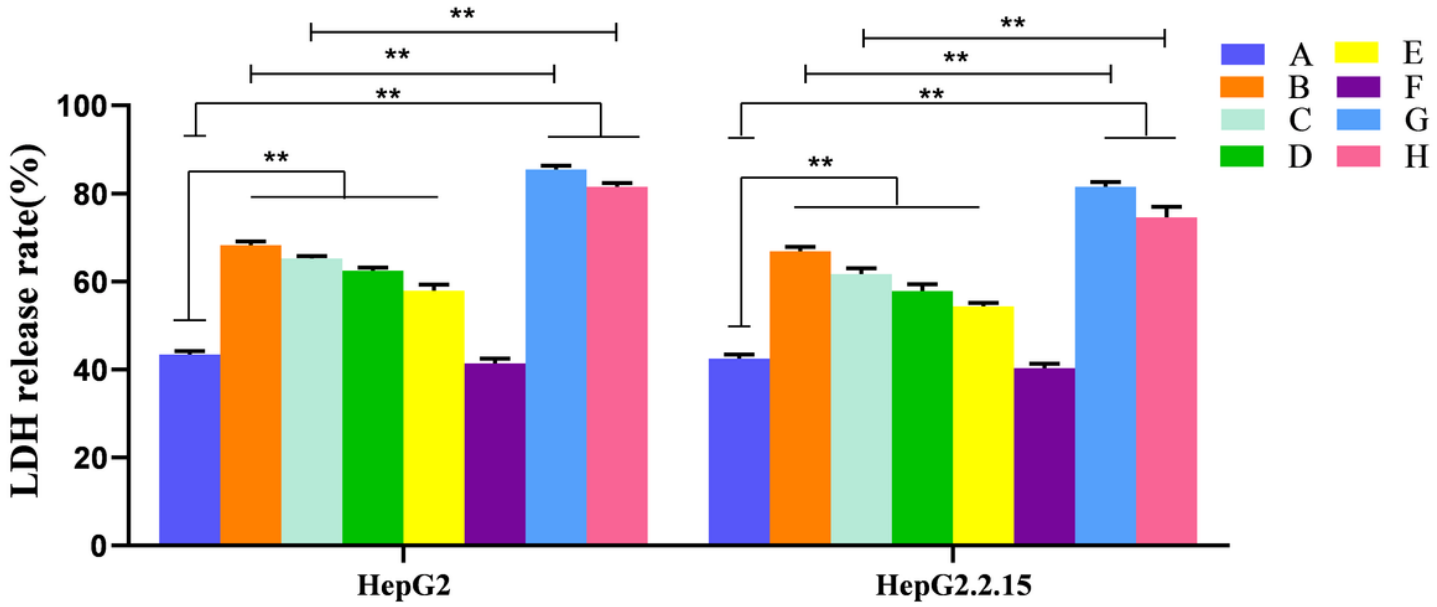

Figure 13

The effect of each drug group on the release rate of lactate dehydrogenase (LDH) in HepG2 and HepG2.2.15 cells (`x±s□n=3).A. blank group; B. PPI; C.Cur; D. sorafenib; E. Erastin; F. Ferrostatin-1; G. PPI+ sorafenib; H. Cur+ Sorafenib; **P<0.01, *P<0.05.

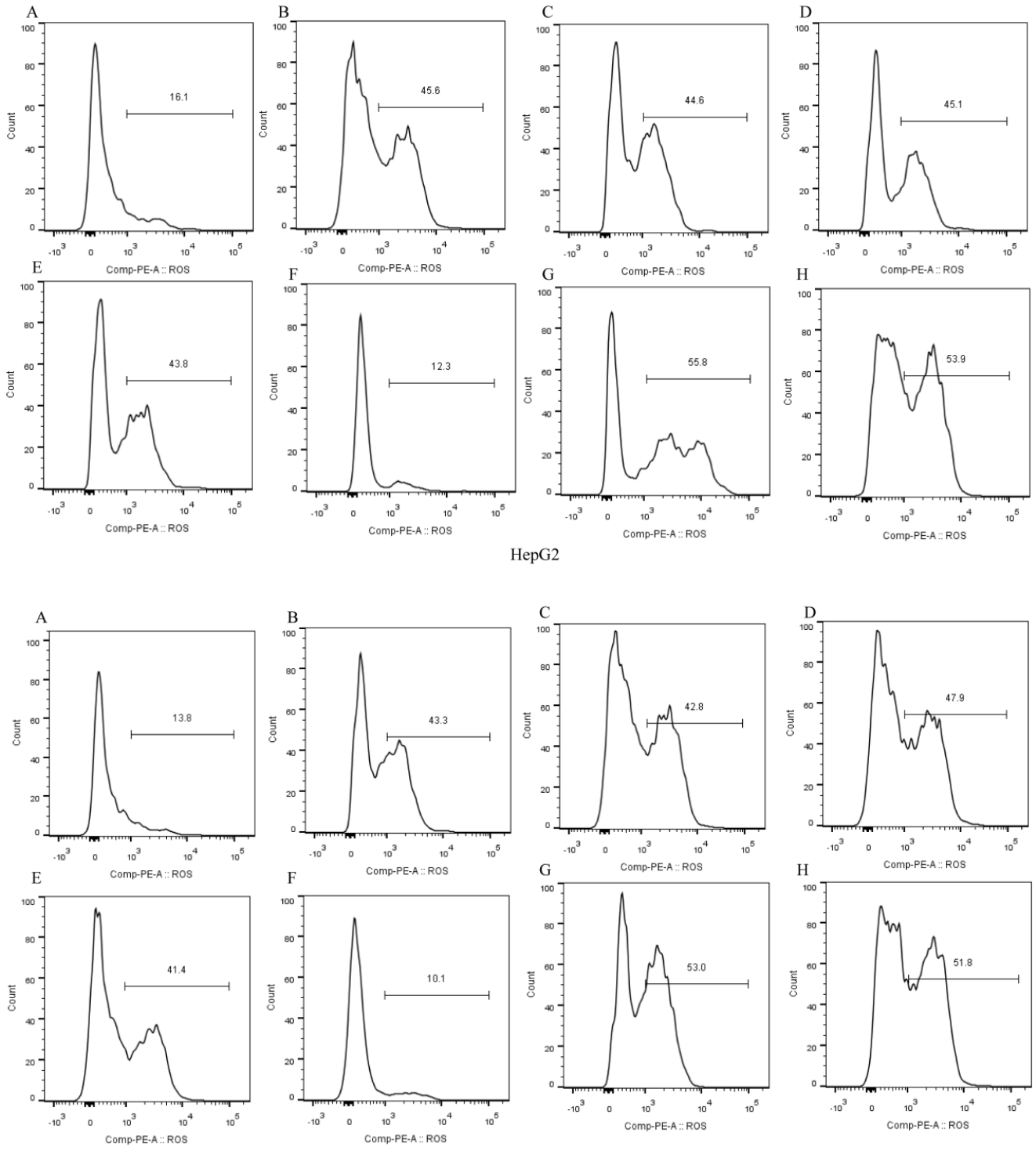

Figure 14

The effect of each drug group on the intracellular ROS levels of HepG2 and HepG2.2.15

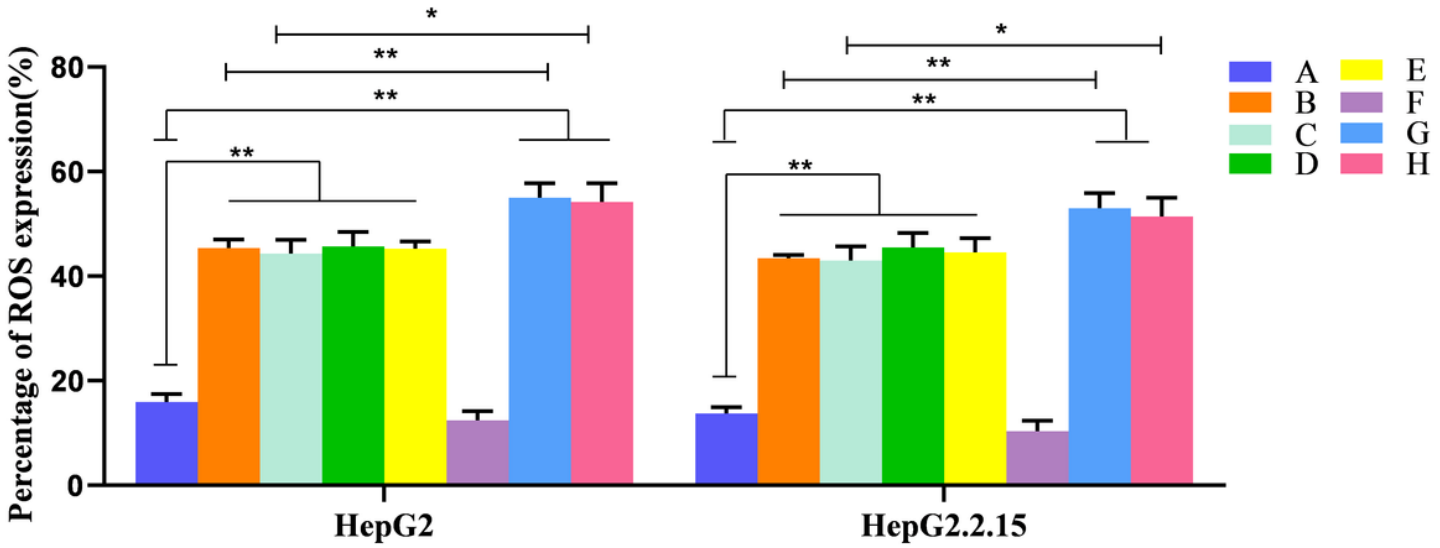

Figure 15

Detection results of ROS levels in HepG2 and HepG2.2.15 cells (`x±s□n=3).A. blank group; B. PPI; C.Cur; D. sorafenib; E. Erastin; F. Ferrostatin-1; G. PPI+ sorafenib; H. Cur+ Sorafenib; **P<0.01, *P<0.05.

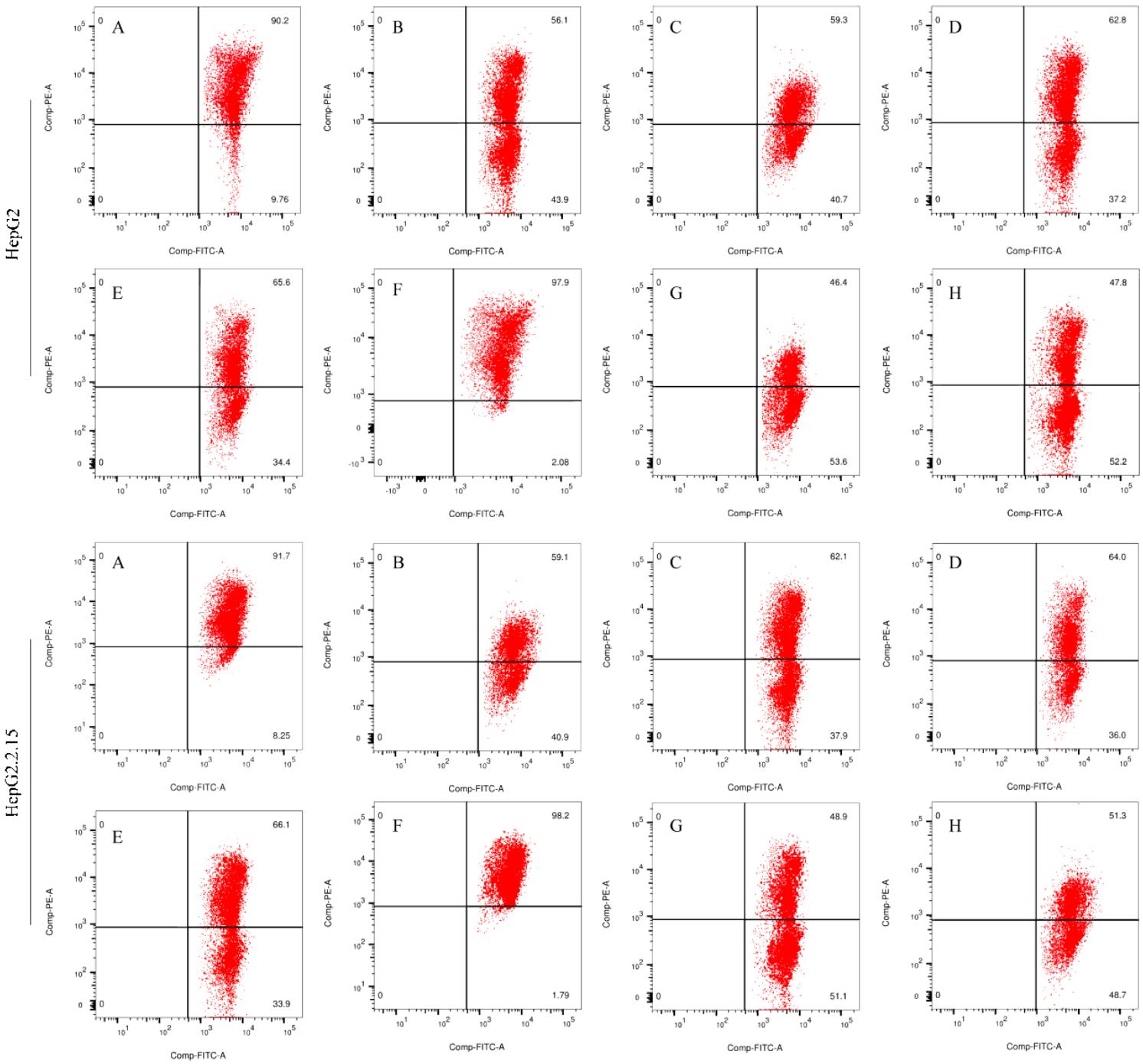

Figure 16

The effect of each drug group on the mitochondrial membrane potential of HepG2 and HepG2.2.15 cells.A. blank group; B. PPI; C.Cur; D. sorafenib; E. Erastin; F. Ferrostatin-1; G. PPI+ sorafenib; H. Cur+ Sorafenib

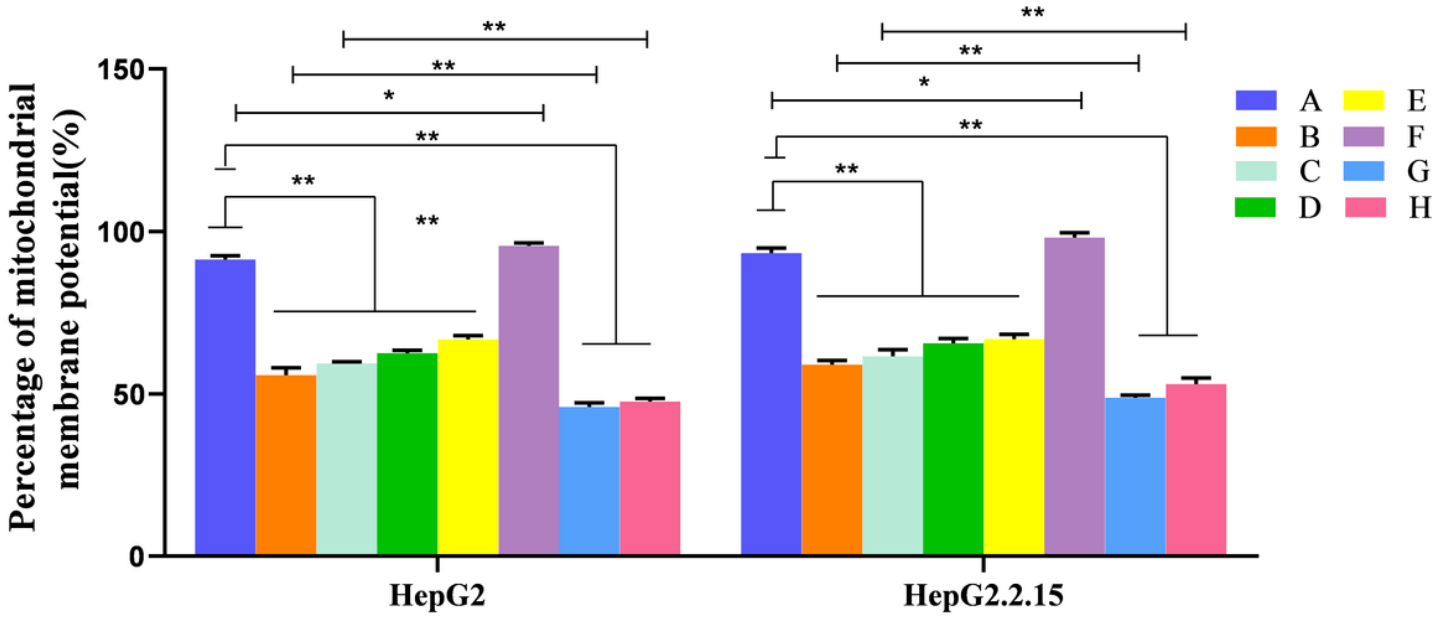

Figure 17

Detection results of mitochondrial membrane potential of HepG2 and HepG2.2.15 cells (`x±s，n=3).A. blank group; B. PPI; C.Cur; D. sorafenib; E. Erastin; F. Ferrostatin-1; G. PPI+ sorafenib; H. Cur+ Sorafenib; **P<0.01, *P<0.05.

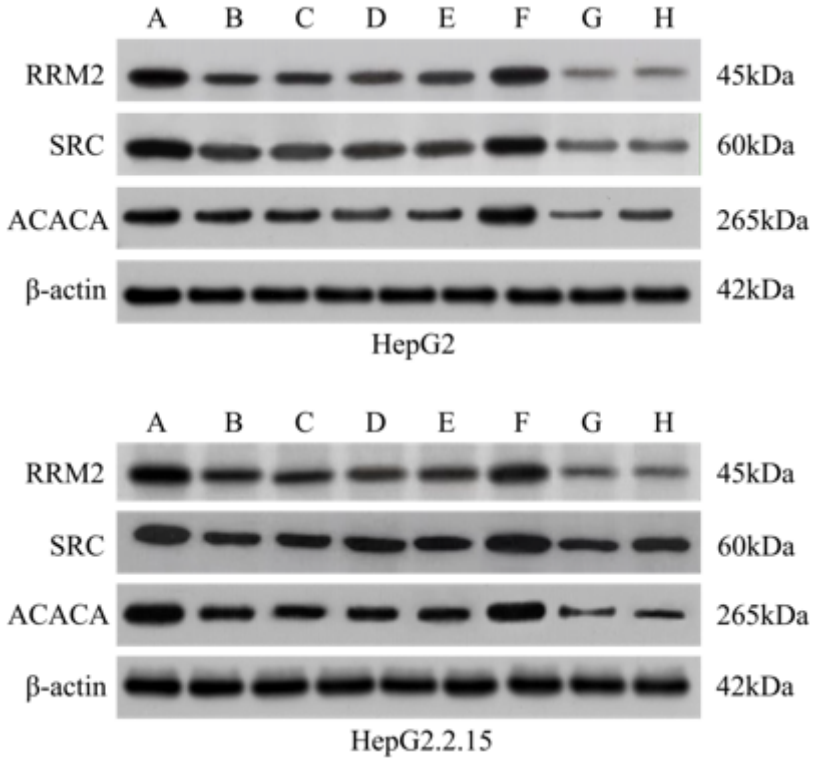

Figure 18

The effect of each drug group on HepG2 and HepG2.2.15 cell RRM2, SRC, ACACA protein expression electrophoresis.A. blank group; B. PPI; C.Cur; D. sorafenib; E. Erastin; F. Ferrostatin-1; G. PPI+ sorafenib; H. Cur+ Sorafenib

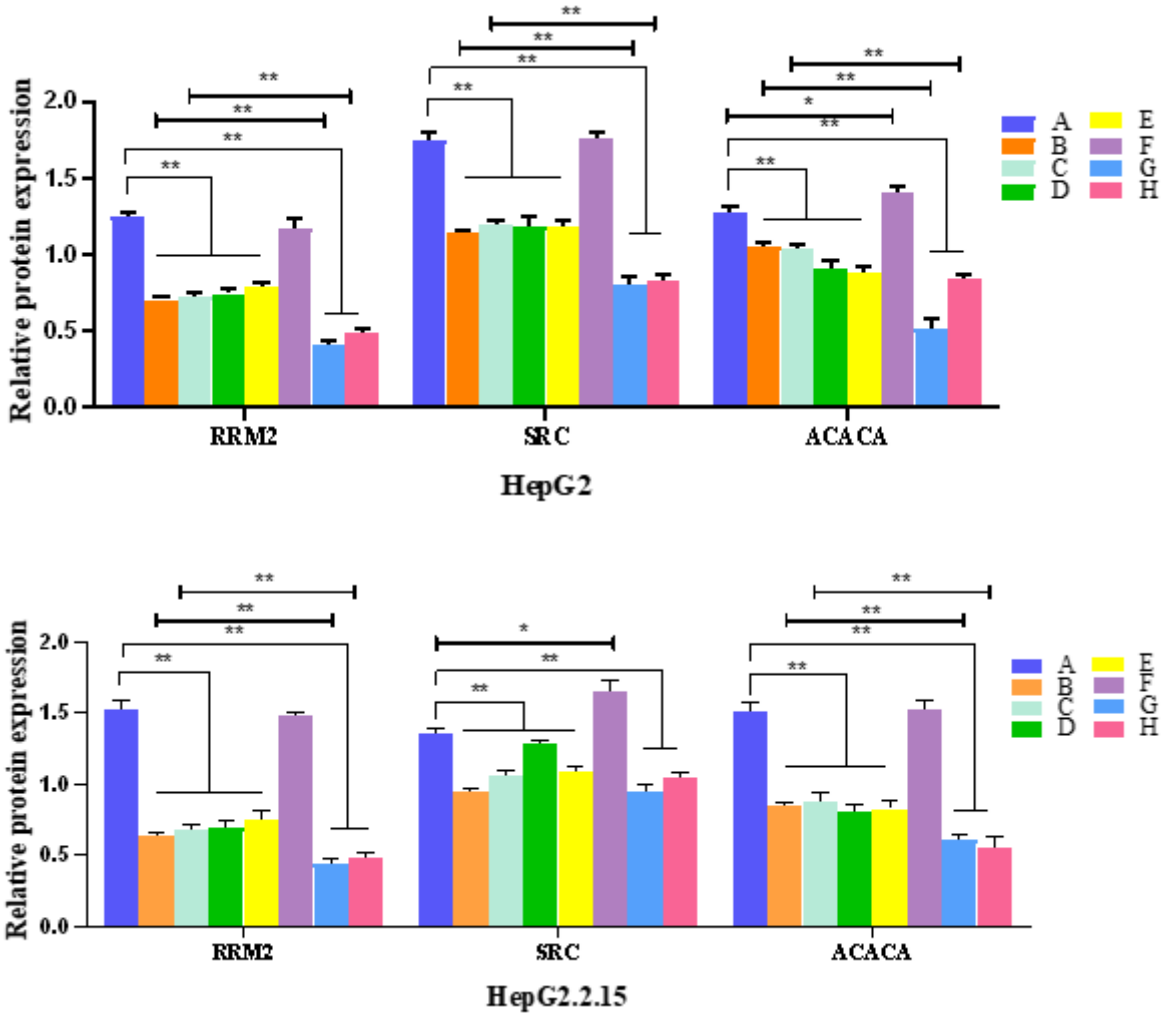

Figure 19

The effect of each drug group on the expression of RRM2, SRC and ACACA protein in HepG2 and HepG2.2.15 cells (`x±s□n=3).A. blank group; B. PPI; C.Cur; D. sorafenib; E. Erastin; F. Ferrostatin-1; G. PPI+ sorafenib; H. Cur+ Sorafenib; **P<0.01, *P<0.05.